Clean Technologies and Environmental Policy
https://doi.org/10.1007/s10098-023-02656-3

ORIGINAL PAPER

Dynamic modeling and techno-economic assessment of hybrid renewable energy and thermal storage systems for a net-zero energy greenhouse in South Korea

Misbaudeen Aderemi Adesanya[1] · Abdulfatai Olatunji Yakub[2] · Anis Rabiu[1] · Abdulhameed Babatunde Owolabi[2,3] · Qazeem Opeyemi Ogunlowo[1,4] · Abdullahi Yahaya[2] · Wook-Ho Na[5] · Min-Hwi Kim[6] · Hyeon-Tae Kim[7] · Hyun-Woo Lee[1,5]

Received: 20 July 2023 / Accepted: 26 October 2023

Abstract

The implementation of hybrid renewable energy and thermal energy storage systems (HRETESSs) in greenhouses holds great promise in terms of greenhouse gas emission reduction, enhanced efficiency, and reliability of agricultural operations. In this study, numerical and experimental studies were conducted on a greenhouse integrated with HRETESSs in South Korea. The system consisted of solar thermal (ST) collectors, photovoltaic thermal (PVT) collectors, thermal energy storage, and heat pump systems. The performance analysis of the HRETESSs in various locations across South Korea was conducted using a validated TRNSYS model, which was calibrated through experimental measurements. RETscreen software was utilized to perform the techno-economic evaluation of the HRETESSs. Across all the cities studied, the HRETESSs achieved an average contribution of 43% and 20% toward meeting the thermal and electrical loads, respectively, resulting in an annual gross reduction of 4326–5157 tons of CO_2. Moreover, the heat injection into the borehole thermal energy storage (BTES) from the ST and PVT collectors increases the contribution of the BTES to the greenhouse load.

✉ Hyun-Woo Lee
whlee@knu.ac.kr

1 Department of Agricultural Civil Engineering, College of Agricultural and Life Sciences, Kyungpook National University, Daegu 41566, South Korea

2 Department of Convergence and Fusion System Engineering, Kyungpook National University, Sangju 37224, South Korea

3 Regional Leading Research Center for Smart Energy System, Kyungpook National University, Sangju 37224, South Korea

4 Department of Agricultural and Bioenvironmental Engineering, Federal College of Agriculture Ibadan, PMB 5029, Ibadan, Nigeria

5 Smart Agriculture Innovation Centre, Kyungpook National University, Daegu 41566, South Korea

6 Renewable Thermal Convergence Laboratory, Korea Institute of Energy Research, 152 Gajeong-ro, Yuseong-gu, Daejeon 34129, South Korea

7 Department of Bio-Industrial Machinery Engineering, Gyeongsang National University, Jinju 52828, South Korea

Published online: 22 November 2023

Graphical Abstract

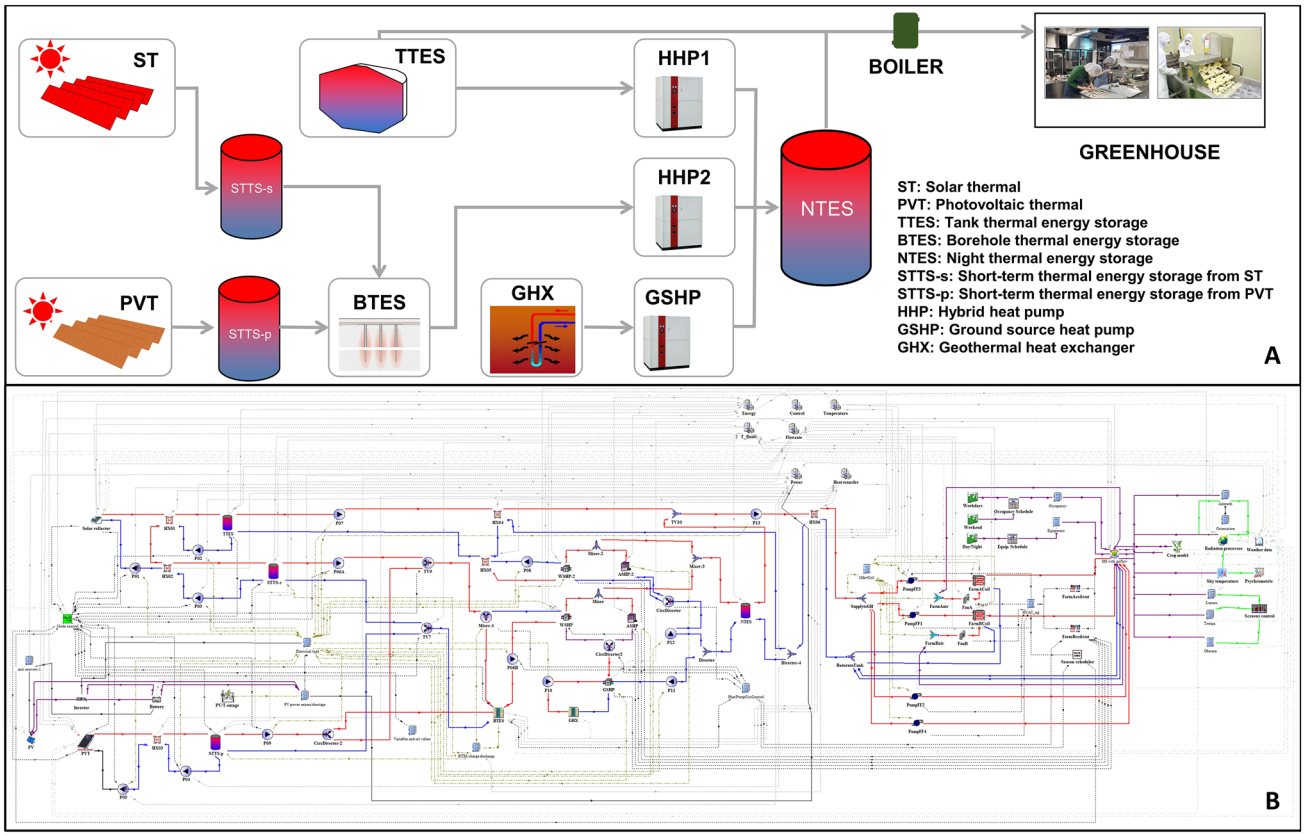

Keywords Greenhouse · Hybrid renewable energy · Thermal energy storage · TRNSYS · RETscreen · Techno-economic assessments

Abbreviations

ALS	Annual life savings
BC	Benefit cost
CO_2	Carbon dioxide
DC	Direct current
DGHS	Duct ground heat storage
GHX	Ground heat exchanger
GSHP	Ground source heat pump
HRETESSs	Hybrid renewable energy and thermal energy storage systems
HWP	Hot-water pipes
IRR	Internal rate of return
LCOE	Levelized cost of energy
NPV	Net present value
NTES	Night thermal energy storage
O&M	Operation and maintenance
PV	Photovoltaic
PSF	Purme social farm
SR	Solar radiation
STTS	Short-term thermal storage
STTS-p	Short-term thermal storage for photovoltaic collectors
TES	Thermal energy storage
ASHP	Air source heat pump
BTES	Borehole thermal energy storage
COP	Coefficient of performance
DHW	Domestic hot water
FCU	Fan coil units
GHG	Greenhouse gas
HHP	Hybrid heat pump
HX	Heat exchanger
KRW	Korean won
LTTS	Long-term thermal energy storage
NSE	Nash–Sutcliffe coefficient
NZEG	Net-zero energy greenhouse
PID	Proportional integral and differential controller
PVT	Photovoltaic combined with solar thermal
RES	Renewable energy system
ST	Solar thermal

STTS-s	Short-term thermal storage for solar collectors
TTES	Tank thermal energy storage

Introduction

Due to the increasing global energy demand and the rapid depletion of traditional fuel sources, there is an urgent need to investigate alternative energy sources (Ushamah et al. 2022). The impact of fossil fuels on the ecosystem has become increasingly evident, necessitating a shift toward sustainable energy alternatives that do not rely on finite resources. The shift toward sustainable energy plays a vital role in mitigating the detrimental impact of fossil fuels on the climate and realizing sustainable development goals (Anifantis et al. 2017). Therefore, it is vital to invest in renewable energy systems (RESs) and embrace them as a key element of the energy mix for a greener and more sustainable future (Chaima et al. 2023).

Economic policies, such as those pertaining to future agricultural expansion, are essential for domestic economies in both the industrial and commercial sectors (Nadi and Campbell 2023). Climate change, which impacts agricultural output and food production, must be addressed by the agriculture industry and investing in agriculture is of utmost importance to guarantee food security and meet the demands of the world's growing population (Yakub et al. 2022). Greenhouses are crucial production systems that can address the challenges of food security and reduce the ecological impact of global food systems. They offer a viable solution without compromising the nutritional requirements of expanding urban populations (Gorjian et al. 2021).

Due to its high energy consumption within the agricultural sector, incorporating greenhouses into the energy transition strategy has become imperative (Ouazzani Chahidi and Mechaqrane 2023) and given the longstanding emphasis on solar energy in net-zero energy greenhouse (NZEG) implementation, RESs such as photovoltaic (PV), solar thermal (ST), and photovoltaics combined with solar thermal (PVT) are viable options for directly harnessing solar energy to mitigate the increasing heating and cooling expenses in the greenhouse sector (Calise et al. 2023).

Compared to countries like the USA and Canada, South Korea ranks among the top oil-consuming nations globally, yet its utilization of RESs remains relatively low (Lee 2009). To address this concern, the South Korean Government has taken steps to increase the share of RESs to 20% by 2030 (Lee and Xydis 2023) and attaining these ambitious goals require new measures and policy aimed at reducing carbon dioxide (CO_2) emission (Chew et al. 2023). One of these measures in South Korea involve offering installation expense subsidies ranging from 30 to 80% (MOTIE 2017). With the subsidy program, ST, PV, and geothermal heat have shown that they are more economically viable compared with fuel cells, and it is possible to make other energy sources economically viable through optimization (Choi et al. 2018).

Due to various barriers, the adoption of RESs in greenhouses in South Korea has been limited and lacks widespread implementation, resulting in a scarcity of reported studies. In 1998, the first simulation of solar heating systems for a coupled greenhouse-residential building in South Korea was conducted using TRNSYS (Chung et al. 1998). Subsequently, a few pilot models have been proposed, albeit with limited verification. One of such studies was the use of hybrid heat pump (HHP), pellet boiler, and ST for heating a 90 m^2 greenhouse in Gangwon-do (Lee et al. 2021). While the experiment's main discovery revealed no notable discrepancies in the combined thermal efficiency, the system managed to reduce costs by 27.7% in comparison to traditional fossil fuel boilers.

Numerous studies conducted worldwide have investigated various configurations of hybrid renewable energy and thermal energy storage systems (HRETESSs) to enhance the utilization of solar energy in greenhouses. For example, in Canada, the performance of two distinct borehole thermal energy storage (BTES) systems, one operating at low temperature and the other at high temperature, was analyzed using TRNSYS (Semple et al. 2017). The coefficient of performance (COP) for the two systems was 2.9 and 21.7, respectively. Similarly, Ridder et al. examined the feasibility of a long-term thermal energy storage (LTTS) system explicitly designed for greenhouse horticulture in Europe (Ridder et al. 2020). By employing different simulation controls, they achieved a reduction in heating energy costs ranging from 0.50 to 6.15 m^2/year, along with a decrease in CO_2 emissions of 700 g/m^2/year. Engler and Krarti performed a systematic analysis for enhancing the energy efficiency of indoor farming facilities while incorporating RES in different states in the US (Engler and Krarti 2022). The results demonstrated that life cycle cost optimal designs consistently reduce annual energy consumption by up to 65%. In China, a typical solar greenhouse was transformed into NZEG by combining passive insulation and PV technology (Jiang et al. 2023). Various retrofit options were analyzed through PVsyst software and the PV panels with checkerboard demonstrated the highest comprehensive score with 5.23 years payback period.

In the context of analyzing economic and environmental feasibility of solar heating systems in sectors unrelated to greenhouse applications, the RETscreen tool has been employed in various studies. Pan et al. examined the development of a multiple energy complementation system for Chongming's energy system in South Korea (Pan et al. 2017). Alsantali and Almarshoud performed a power quality

and economic analysis of a building-integrated PV system across five cities in Saudi Arabia, resulting in a levelized cost of energy (LCOE) of 0.095 SAR/kWh over 10 years (Alsantali and Almarshoud 2023). In Bangladesh, Datta et al. investigated the financial and environmental impacts of installing rooftop PV systems in commercial buildings and employed NASA climatic data for economic performance simulation (Datta et al. 2020). The project was financially attractive, yielding a net present value (NPV) of $756,896 and an internal rate of return (IRR) of 14.2%. Similarly, Farooq and Zhang performed techno-economic assessment on two different configurations of ST collectors and thermal energy storage (TES) systems for a residential building (Farooq and Zhang 2022).

A notable distinction in the current study is the evaluation of the system's performance using real-life monitoring data, specifically applied to the greenhouse. Also, the modeling method is unique because it combines the greenhouse and the HRETESSs into a single TRNSYS model. This makes it possible to analyze separately how the greenhouse load is affected by TES, heat pumps, and solar thermal systems. Moreover, since the construction of the examined HRETESSs and the associated greenhouse was originally planned without the inclusion of this study, we are currently unable to make fundamental design modifications. Nonetheless, we consider this study highly significant due to the comprehensive comparison between the real-life performance of the HRETESSs and the developed model. As a result, the validated TRNSYS model serves as a solid basis for predicting the performance of large-scale HRETESSs with different TES and heat pump systems in various regions of South Korea. The findings of this study are anticipated to contribute to the advancement of sustainable energy production and greenhouse cultivation practices in South Korea. The remaining sections of the paper are structured as follows: "Methodology" section describes the methodology; "Results and discussion" section presents the results and discussion; and finally, "Summary and conclusions" section provides a summary and conclusion.

Methodology

Description of the case study

The investigated NZEG, Purme social farm (PSF), is located at Ohak-dong, Yeoju-si, Gyeonggi-do, South Korea. The PSF has a land area of 11,800 m^2, which includes a multispan glass greenhouse, cafe, crop processing room, and educational institute. PSF is made of low-tech plastic greenhouses of different sizes for growing strawberries, watermelons, cucumbers, and pumpkins. It was renovated into a self-sufficient glass greenhouse to grow cherry tomatoes and integrated with HRETESSs, (Fig. 1). The specifications including ST collectors, PVT collectors, heat pumps, and TES systems are presented in Supplementary Table 1. The TES systems consist of two LTTSs and three short-term thermal storages (STTS-s). The LTTSs are subdivided into the tank thermal energy storage (TTES) and BTES, while

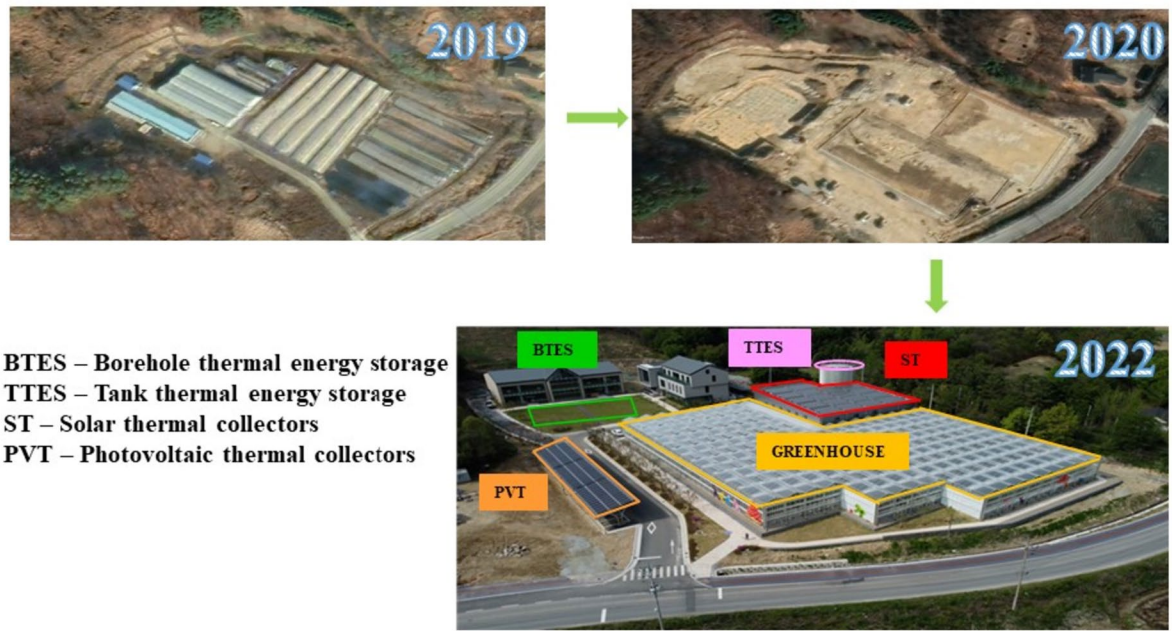

Fig. 1 Evolution of the case study

the STTS-s are made of the night thermal energy storage (NTES), short-term thermal storage for ST collectors (STES-s), and short-term thermal storage for PVT collectors (STES-p). Notably, the heat pumps are composed of six units: four HHPs and two ground source heat pumps (GSHPs). Two of the four HHP units use a heat source from the TTES (HHP1), while the other two use heat sources from the BTES (HHP2).

The BTES utilizes the detached open ground between the cafe and the educational institute, while the TTES utilizes the compartment beside the crop processing room. The ST is installed on the roof of the crop processing room, while the PVT is installed in the parking lot. The ST and PVT are inclined at 5.76° and 45° toward the south for maximum solar radiation (SR) interception. The inclination angles of the ST and PVT systems were meticulously designed to optimize energy yield from each system. The ST system is dedicated to the production of thermal energy through the capture of SR. Its inclination angle of 5.76° corresponds to the latitude of the experimentation site. This latitude tilt angle is strategically chosen to align the ST collector's surface almost perpendicularly with the sun's rays during the winter months when the sun reaches its lowest declination. This alignment maximizes heat collection precisely when heating demands tend to be at their peak. Conversely, the PVT system serves a dual purpose, generating both electricity and thermal energy. To achieve the most efficient balance between these objectives, the PVT is inclined at an angle of 45°, corresponding to the azimuth of the experimentation site. This orientation ensures the PVT collectors receive sunlight throughout the day, optimizing SR interception for both thermal energy collection and electricity generation.

The experimental site experiences a humid continental climate characterized by winter temperatures dropping as low as − 19 °C and summer temperatures peaking at 35 °C, as shown in Fig. 2, while SR ranges between 10 and 3620 kJ/hm^2 with peak values in May and June. This ambient variation creates an imbalance in the energy consumption pattern of the greenhouse, necessitating the need for TES systems.

System description and operation mechanism

The HRETESSs system installed in Yeoju-si, South Korea, offers heating and cooling capabilities to the 3942-m^2 greenhouse. As depicted in Fig. 3, the collected thermal energy from the ST collector is initially stored in the TTES, and once the desired TTES temperature is achieved, it is subsequently transferred to the STTS-s. The PVT system generates both thermal and electrical energy, with the former being stored in the STTS-p and the latter in a battery pack. The accumulated thermal energy in the TTES is directly supplied to the greenhouse during early winter, while the accumulated thermal

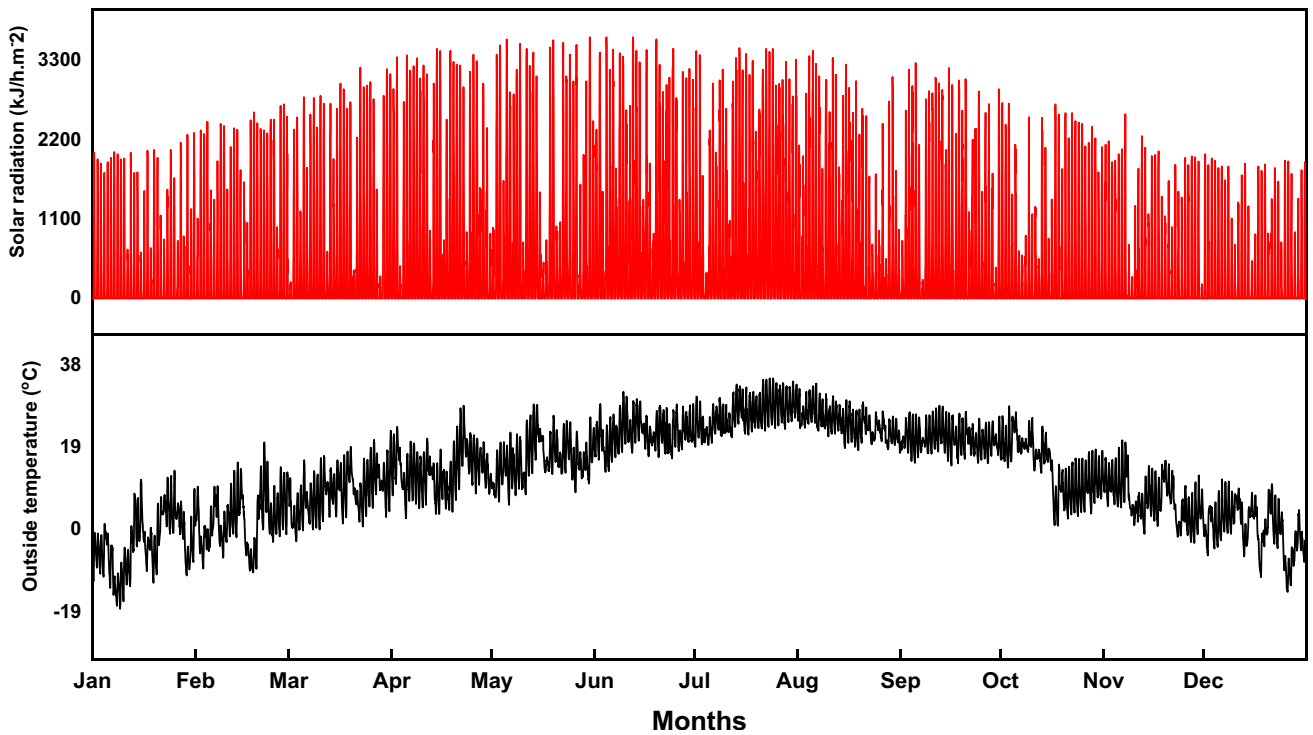

Fig. 2 Outside weather conditions of Yeoju-si, South Korea

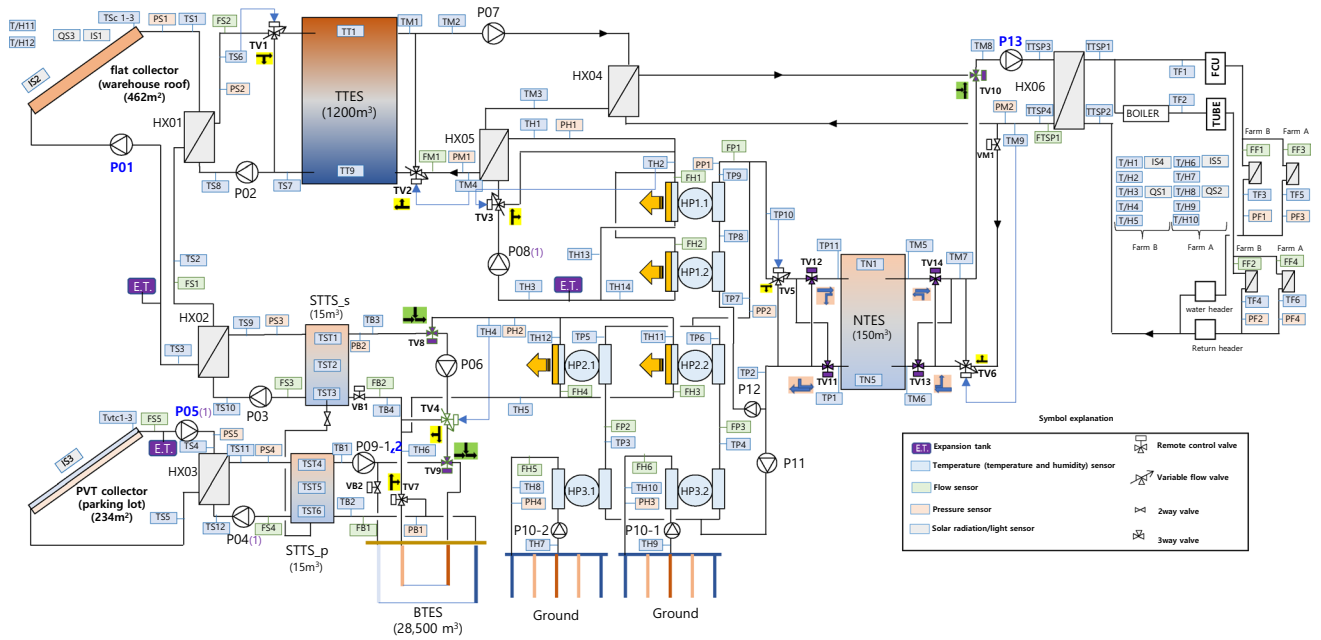

Fig. 3 Overview of hybrid renewable energy and thermal energy storage systems

energy in the STTS-s and STTS-p is injected into BTES. In cases where the TTES temperature alone is insufficient for direct supply, HHP1 utilizes thermal energy from the TTES and stores the generated heat in the NTES. Similarly, the stored thermal energy in the BTES serves as a heat source for HHP2, which provides thermal energy and subsequently stores it in the NTES. HHP1 and HHP2 operate as air-source heat pumps (ASHP) during the summer to supply cold water, which is stored in the NTES. The GSHP is utilized for heating and cooling depending on the greenhouse condition. The thermal energy in the NTES is distributed to the greenhouse through hot-water pipes (HWPs) and fan-coil units (FCUs). In the event of extreme weather conditions or sudden failure of the heat pump systems to provide thermal energy, an electric boiler serves as a backup.

During the experimentation at PSF, specialized sensors were strategically placed within the HRETESS thermal energy flow, as part of the data collection process. Supplementary Table 2 provides details regarding the characteristics of the installed sensors and Eq. 1 was used to calculate the experimental thermal energy produced within the HRETESSs and the greenhouse.

$$Q = \dot{m} \times C_p \times \Delta t \tag{1}$$

where Q is the amount of energy consumed (kWh); $\dot{m}$ is the mass flow rate (L/min); C_p is the specific heat capacity of water (kJ/kg C), and Δt is the changes in water temperature (C).

Modeling in TRNSYS

The TRNSYS simulation interface allows for the modeling of any system using the standard library components or user-defined nonstandard components called "Types" (Ogunlowo et al. 2022). The modeling of the HRETESSs and greenhouse was accomplished with several loops of subsystems using the standard TRNSYS library components. The description, mathematical relation, and control of each subsystem is detailed in the following sections:

Solar collector loop

The solar collector loop is comprised of the ST and PVT loops. The ST loop includes the ST (Type 1C), inverter pump (Type 11), single-speed pump (Type 114), heat exchanger (HX) (Type 91), vertical and cylindrical storage tank (Type 1534), proportional integral and differential (PID) controller (Type 23), ON/OFF controller (Type 165), and equation editors. The ST collectors receives SR and transfers heat to the propylene glycol aqueous solution running through it, then transfers the absorbed energy to the TTES via HX01. If the water stored in the TTES has reached the desired temperature, the excess heat absorbed from the ST is pumped into STTS-s via HX02. The flowchart for the ST loop is depicted in Fig. 4. The recorded weather data needed for the dynamic simulation were all added into the data reader (Type 9e), and the corresponding parameters were selected. The required fixed parameter for other components in the ST loop is listed in Supplementary Table 3.

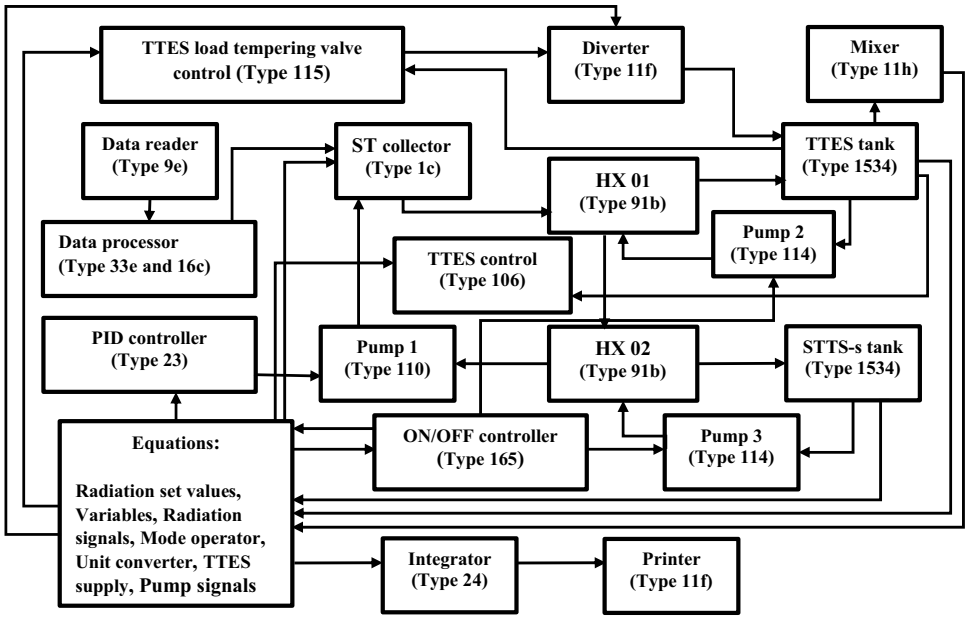

Fig. 4 Solar collector loop flowchart

Type 1c models the thermal performance of a flat-plate ST collector using a quadratic efficiency equation. The coefficients were obtained from the standard performance test of the SNG-CS1 model conducted by the Korea Laboratory Accreditation Scheme. The coefficients plot the collector efficiency to the ratio of the temperature differential to the SR. The effects of the normal SR incidence were modified using optical mode 3 in the parameter tab of Type 1c that permits transversal and longitudinal incident angle modifiers at different incidence angles to be read by the user-supplied data. The algorithm of the ST collector efficiency for Type 1c is based on the Hottel–Whillier equation (Duffie and Beckman 1982), which is written as:

$$\eta_{\text{collector}} = \eta_0 - \alpha_1\left[\frac{(T_m - T_a)}{G}\right] - \alpha_2\left[\frac{(T_m - T_a)^2}{G}\right], \tag{2}$$

where $\eta_{\text{collector}}$ is the ST efficiency, η_0 is the optical efficiency, α_1 and α_2 are the first- and second-order coefficient heat losses, T_m is the collector temperature °C, T_a is the outside temperature (°C); and G is the SR (kJh^{-1} m^{-2}).

Two major controls were adopted for Type 1c: Type 23 PID controller and Type 165 differential controller. Type 23 prevents the overheating of the ST collector by ensuring a positive flowrate when the error between the setpoint and the collector's output temperature is negative. This is achieved with a negative gain constant for the PID parameters. The minimum allowable incident SR for operating ST determines the ON/OFF signal of the PID control expressed in Eqs. (3)–(5), while the TTES outlet temperature from the source side plus a constant determines the PID setpoint, as expressed in Eqs. 6 and 7. Type 165 monitors the SR incident on the ST collector and the outlet temperature from the ST collector, TTES (source side), and STTS-s (source side). The outlet temperature from the ST is connected as the upper input temperature, the outlet temperature from the source side of the TTES is connected as the lower input temperature, and the TTES node 1 temperature is connected as the monitored temperature of Type 165. The pump for the ST switches ON when the collector's temperature is 10 °C above the temperature of the bottom of the TTES and continues to operate until the temperature falls 5 °C below the temperature of the TTES.

$$\gamma_{\text{PID}_{\text{on/off}}} = \text{AND}\big(\text{EQL}\big(\gamma_A, 1\big), \text{EQL}\big(\gamma_B, 1\big)\big), \tag{3}$$

$$\gamma_A = \text{GT}(\text{IS2}, I\text{min1}), \tag{4}$$

$$\gamma_B = \text{GT}(\text{IS2}, I\text{min2}), \tag{5}$$

$$\gamma_{\text{PID}_{\text{setpoint}}} = \text{EQL}\big(\gamma_C, 1\big) \times \text{TT9}, \tag{6}$$

$$\gamma_C = \text{AND}(\text{EQL}\Big(\gamma_{\text{PID}_{\text{on/off}}}, 1\Big), \text{EQL}\big(\gamma_D, 1\big)) \tag{7}$$

where γ_A is the signal to start heat absorption from the ST collector; γ_B is the signal to stop heat absorption from ST; γ_C is the signal to start heat rejection from the ST collector to the TTES; γ_D is the signal for Type 165 to begin operation; IS2 is the inclined incident SR at the slope of ST (kJ h^{-1}m^{-2}); Imin1 is the minimum allowable IS2 for heat collection from ST (1080 kJ h^{-1}m^{-2}); Imin2 is the minimum allowable IS2 to stop heat collection from ST

(720 kJ $h^{-1}m^{-2}$); and TT9 is the bottom node temperature of the TTES (°C).

Type 1534 models a constant volume storage tank filled with fluid. Heat is transferred into and out of the tank between the mixing of the fluid streams and the storage fluid. The tank is divided into isothermal nodes, and the fluid interacts with the environment through the defined thermal losses specified in the parameter of the component. The thermal losses from the top, bottom, and edges are defined using Eqs. (A.1)–(A.3) in Appendix A, while the temperature at the nodes is solved using a differential equation in Eqs. (A.4) and (A.5) in Appendix A (Solar Energy Laboratory 2018).

Further, the major components of the PV loop are the utility grid (Type 1236), an inverter (Type 48), a battery (Type 549), a PV (Type 190), and a glazed flat plate ST (Type 1348). A propylene glycol aqueous solution is delivered to Type 1346 via a pump and is heated up after absorbing energy (Fig. 5). The heat is then transferred via HX03 to the STTS-p, which is later rejected into the BTES. Type 190 generates direct current (DC), which is stored in Type 549. Type 1236 is a forcing function used to represent the unavailability of the PV to meet the desired electrical load during the simulation. It takes the number of random outages, random number seed, number and start of planned down times, planned down time duration, and minimum and maximum outage length as parameters. Type 48 is a PV charge regulator and inverter that distributes the PV DC power to the battery and converts the DC power to alternating current and distributes it to the load. Type 549 models a lithium-ion battery using the voltage model proposed by Tremblay et al. (2007). The algorithm used in Type 190 is based on the five-parameter equivalent circuit model developed by Duffie and Beckman (1982). It determines the current–voltage characteristics of a single module under different operating conditions using Eq. (A.6) in Appendix A (De Soto et al. 2006).

Similar to Type 1c model, the collector efficiency and off-normal performance of Type 1348 are modeled with quadratic curve-fits from the collector performance test. The incident SR on the PVT array and the outlet temperature from the STTS-p (source side) is controlled with Type 23. The outlet temperature from the PVT is connected as the controlled variable of the PID, the minimum allowable incident radiation for operating the PVT determines the ON/OFF signal of the PID control, and the STTS-p outlet temperature from the source side determines the PID setpoint. Moreover, the pump for the PVT switches ON when the PVT outlet temperature is 10 °C above the temperature of the bottom of the STTS-p and continues to operate until the outlet temperature is 5 °C below the temperature of the STTS-p. The other parameters required for the components of the PVT loop are shown in Supplementary Table 4.

Heat pump and borehole thermal energy storage loop

The heat pump and BTES simulation flowchart are shown in Fig. 6. The loop involves the ground heat exchanger (GHX) (Type 557 and 548), heat pump models (Type 927 and Type 941), and cylindrical storage tank (Type 1534). Type 927 model water–water heat pump and take the heat source from the TTES, BTES, and ground, respectively, while Type 941 models the ASHP. Type 1534 represents the NTES that was connected to the heat pumps in parallel. Unlike TTES, STTS-s, and STTS-p, which are charged by solar energy,

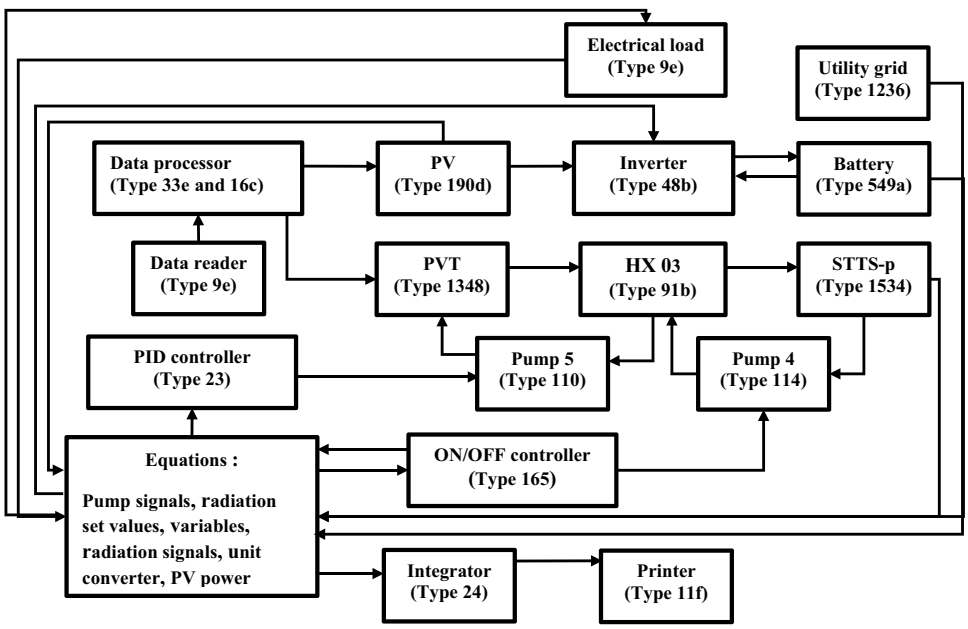

Fig. 5 Flowchart of the photovoltaic solar collector loop

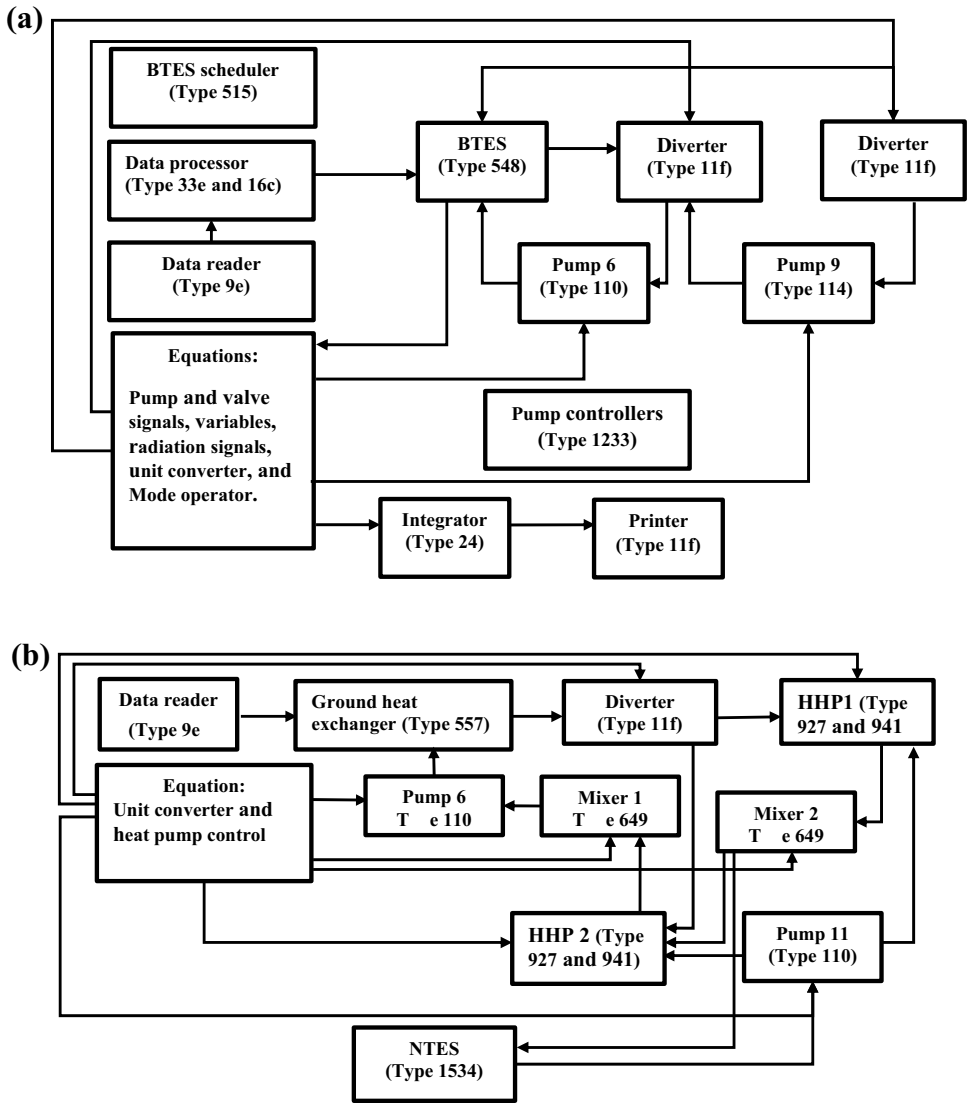

Fig. 6 Flowchart **a** borehole thermal energy storage loop **b** heat pump loop

the NTES was mainly charged using the heat pumps. The multi-tanks in the loops reduce the competition between the heating sources.

The heat pump is operated under two conditions: (1) load and daytime operation of the greenhouse and (2) water temperature conditions. The heat pump is permanently switched OFF after operating continuously for a set time (Hpoptime = 2 h). The source pump of the NTES switches OFF when the inlet temperature at the load side of all the heat pumps becomes greater than the set temperature (Thin = 55 °C) during the heating season. While the load-side pump of the NTES is ON, if the temperature leaving the topmost node of the NTES is less than the greenhouse hot-water demand temperature (Tshmin = 50 °C), the source pump of the NTES switches ON to begin replenishing heat from the heat pumps to the NTES.

Type 548 and Type 557, respectively, represent the BTES and GHX components in the model. The ST and PVT systems heat Type 548 in the summer, while in the winter, it releases heat to HHP2. Both Type 548 and 557 component use the duct ground heat storage (DGHS) algorithm created at the Department of Mathematical Physics, University of Lund (Hellstrom 1989) to model a U-tube vertical GHX that interacts thermally with the ground. With the introduction of the thermal energy systems specialist library 18, Type 557 was changed to Type 548, allowing the DGHS model to function in multiple instances and giving users the flexibility to choose the number of fluids involved in heat rejection or absorption during a simulation. Since the ST and PVT systems are used to inject heat to the BTES, the Type 548 has two fluid inlets. Inlets 1 and 2 are for the ST and PVT

systems, respectively. Using the signals in Eqs. (B.1) and (B.2) in Appendix B, Type 1233 was used to keep an eye on the temperature of the STTS-s and STTS-p. This was done to make sure that the STTS-s and STTS-p could heat the internal or external storage of the BTES on their own or at the same time.

Greenhouse loop

SketchUp software is used for the three-dimensional design of the greenhouse, and the modeling procedure has been detailed in our previous study (Adesanya et al. 2022). The interface of the greenhouse loop contains Type 9e, radiation processor (Type 16c), psychrometer (Type 33e), fictive sky temperature (Type 69b), FCU (Type 753), crop model (Type 780), season scheduler (Type 515), ON/OFF control (Type 108), and pumps (Type 654).

Techno-economic assessment in RETscreen expert software

RETscreen aids decision-makers in swiftly and cost-effectively assessing renewable energy projects, minimizing the expenses and time associated with project identification and evaluation. The software's solar technology project model is widely employed globally for determining energy production, life-cycle costs, and greenhouse gas (GHG) emissions reduction for various systems (Owolabi et al. 2019). When it comes to technical sustainability in engineering, product specification plays a crucial role in determining efficiency and optimal utilization. In this study, a predefined solar technology model was employed, tailored to the thermal energy requirements of greenhouses, across five distinct locations in South Korea. For thorough economic analysis, the RETscreen® Expert software employs economic performance metrics defined by Eqs. (C.1)–(C.4) in Appendix C.

The total investment cost for each system includes all actual expenses, encompassing equipment and installation costs and the sources of income consist of incentives and grants, annual savings, annual capacity savings, annual carbon credit income, and income from GHG reduction. Of this income, annual savings is a significant contributor to the financial performance of the project and is calculated through Eqs. (8–10).

$$\text{Annual savings} = \frac{\text{Energy cost with conventional fuel} - \text{Energy cost with renewable energy systems}}{\text{Energy cost with conventional fuel}} \quad (8)$$

Kerosene was used as the conventional fuel and the energy cost for 100% kerosene utilization is calculated as:

$$= \text{Annual fuel consumption} \times \text{cost of fuel per litre} \quad (9)$$

Also, the energy cost with renewable energy systems is calculated as:

$$= (\text{Total annual power consumption of the renewable energy system PVT power production}) \times \text{cost of electricity per kWh} \quad (10)$$

Statistical index for model evaluation

In this study, the TRNSYS model was verified by comparing its results with the experimental measurements using the Nash–Sutcliffe coefficient (NSE). The NSE provides a measure of how well the simulated data aligns with the experimental data in a 1:1 plot. It ranges from $-\infty$ to 1, with values closer to 1 indicating a higher level of predictive capability for the model. The mathematical equation is defined in Eq. (D.1) in Appendix D.

Results and discussion

The TRNSYS model was run from April to March. This was particularly necessary to ensure comparison between the simulation and the monitored system and allow initial TES in the TTES and BTES. A 5-min simulation time step was utilized to reduce numerical errors, accurately predict the dynamics of the monitored system, and improve the overall accuracy of the simulation results. Several months of data from the monitoring of the real-life performance of the HRETESSs were used to compare the simulated and experimental greenhouse and solar loop, while a period of operation of the heat pump was used to validate the heat pump loop. A typical one-year data from January to December 2021 was used as a comparative assessment of the validated model in different zones in South Korea. Weather data of different cities were downloaded from the Korean Meteorological Administration (KMA 2023).

South Korea is geographically divided into nine provinces, each exhibiting significant variations in climate, topography, and weather patterns (Wikipedia 2021). The division of South Korea into specific zones is based on these variations. To assess the performance of the HRETESSs

Table 1 Climatic conditions of the selected zones

Cities	Total yearly solar radiation (kWh/hm^{-2})	Lowest hourly temperature (°C)	Average monthly low temperature (°C)	Average monthly high temperature (°C)
Yeoju (Experimental site)	1435	− 18.3	− 3.0	26.7
Daejeon	1390	− 17.3	− 1.0	27.8
Chuncheon	1406	− 21.7	− 4.7	27.3
Busan	1588	− 12.2	3.3	26.3
Jeju	1411	− 2.7	6.0	27.8

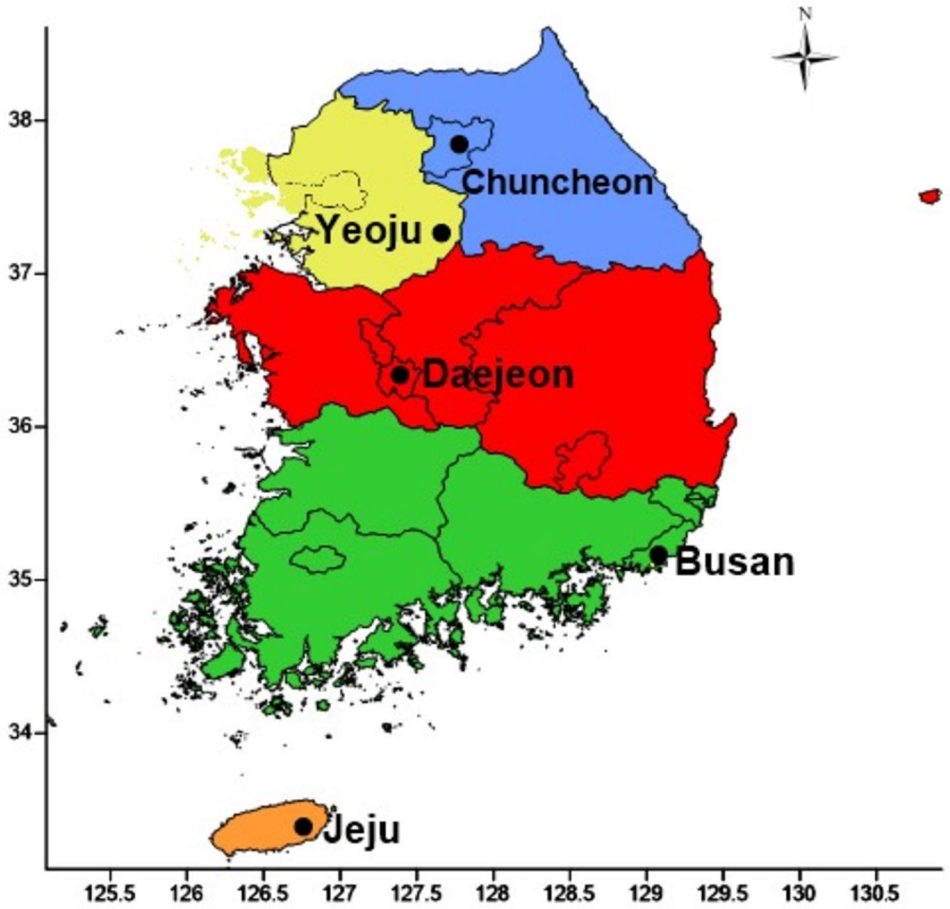

Fig. 7 Map of South Korea divided into different zones

across different provinces, the nine provinces were grouped into five zones, each represented by a chosen city. Table 1 provides weather conditions for these selected zones, and Fig. 7 presents a map of South Korea with these zones color-coded. Specifically, the blue zone represents Gangwon-do province, the yellow zone represents Gyeonggi-do province, the red zone represents Chungcheongnam-do, Chungcheongbuk-do, and Gyeongsangbuk-do provinces, the green zone represents Jeollanam-do, Jeollabuk-do, and Gyeongsangnam-do provinces, and the blue zone represents Jeju province.

Comparative study of the TRNSYS model with the base case

Figure 8 shows the comparison of the monthly collected thermal energy from the ST. As observed, there was a variation in the monthly measured ST collector energy especially in the summer months because experimental data were not stored for some periods due to monitoring system updates and fixing of faulty component parts. However, the overall quality of the ST model performance in comparison to the experiment data is acceptable as the NSE shows a value of 0.87.

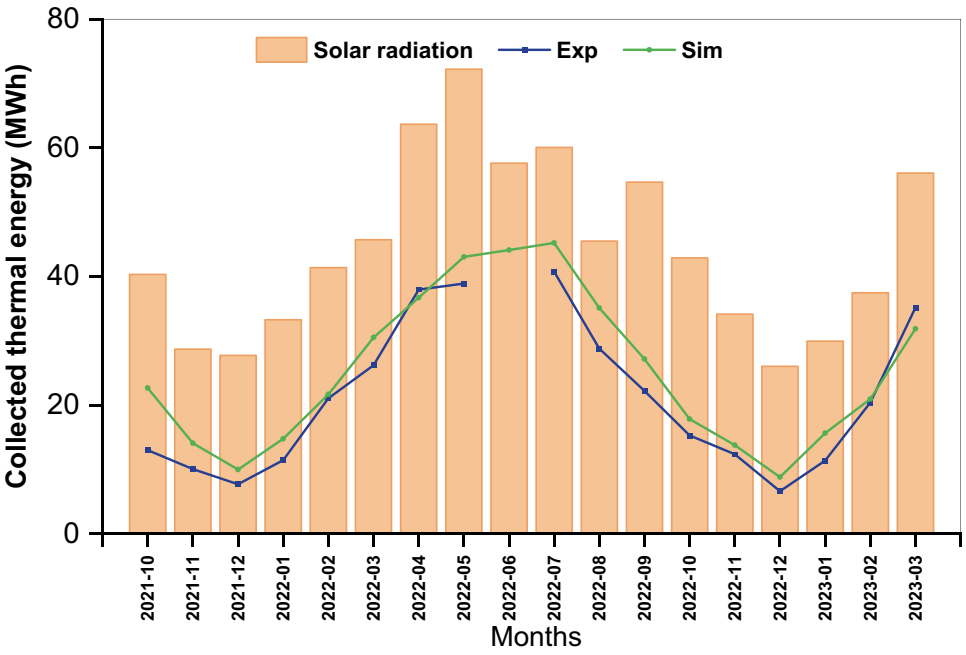

Fig. 8 Comparison of the solar collector thermal energy output based on experimental and simulation data. (Inset: Exp: experiment; Sim: simulation)

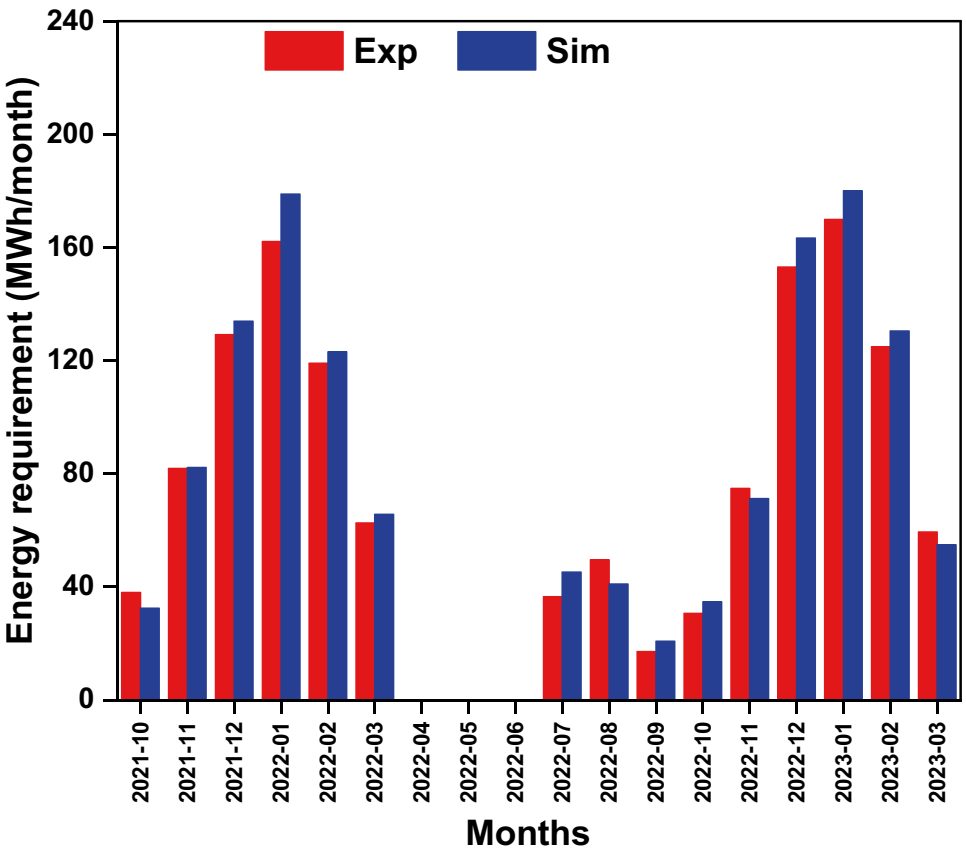

Fig. 9 Comparison of the energy requirements between experiment and simulation (Inset: Exp: experiment; Sim: simulation)

The control of the heating, ventilation, and air-conditioning systems has an impact on the simulated greenhouse load. This control is essential to assessing the energy efficiency of the FCUs and HWPs in maintaining a favorable microclimate while minimizing energy consumption during the experiment. While varying the temperature setpoint for a

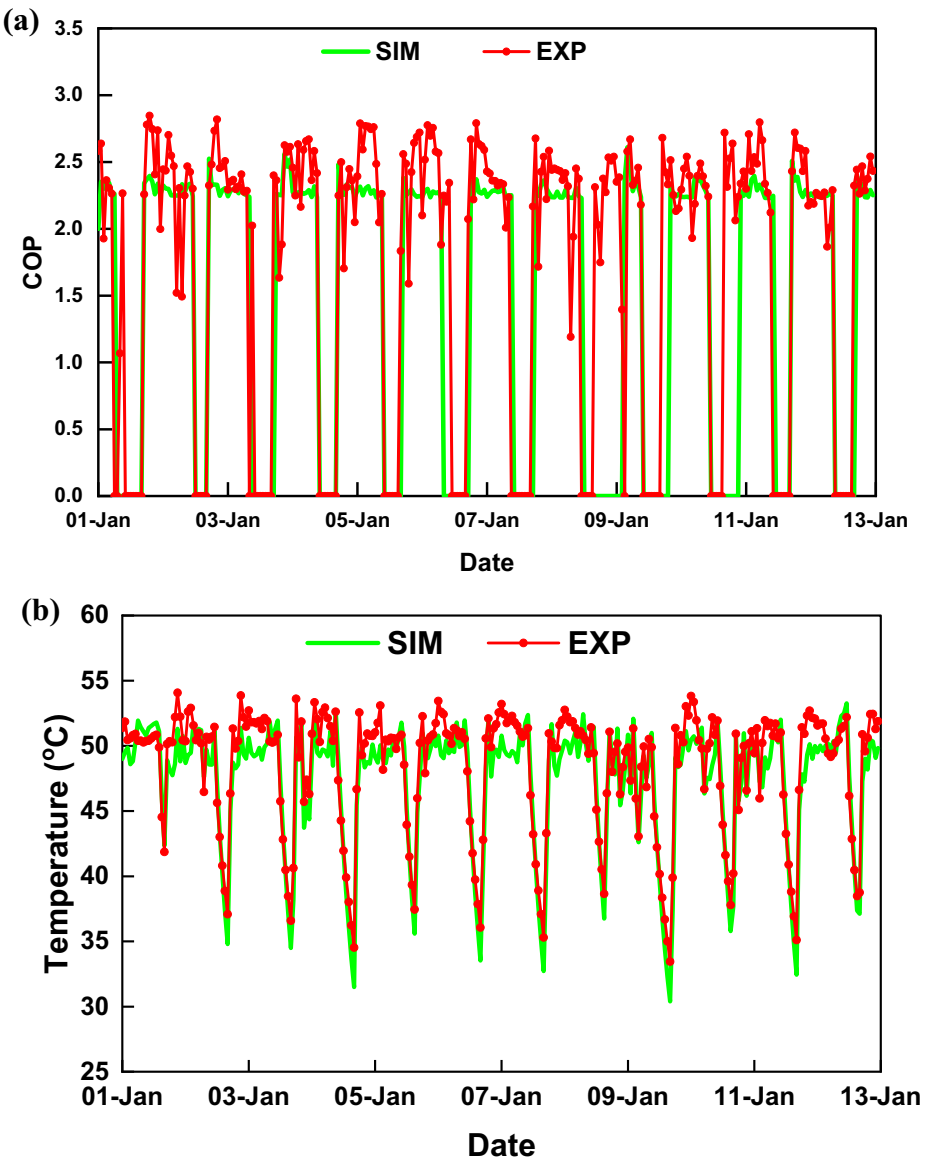

Fig. 10 Heat pump numerical simulation and experimental measurement comparison: **a** COP; **b** load-side output water temperature (Inset: Exp: experiment; Sim: simulation)

growing season between 15 and 20 °C, the total yearly measured and simulated heating load for the first year were 592 and 616 MWh, while the measured and simulated cooling load were 103 and 107 MWh as shown in Fig. 9. During the cooling period, the inability of the FCU to lower the greenhouse temperature to the optimum is due to the low FCU capacity. For instance, there were periods when the greenhouse temperature was as high as 60 °C without cooling in April, May, and June. Overall, the calculated NSE for the greenhouse loop was 0.98.

During the period when the outside temperature was less than 0 °C, HHP1 was being operated. Figure 10a compares the numerical simulation and experimental measured COP of the heat pumps, while Fig. 10b compares the simulated and experimental output water temperature at the load side of the heat pumps. The average simulated COP is constant at ~ 2.27, while the measured COP fluctuates with an average value of 1.83. The amount of energy consumed by the heat pump is a function of its COP and the reason for the constant COP during the numerical simulation is due to the constant power consumption of Type 927. Even though the performance map of the heat pump manufacturer is provided and updated in the external file, Type 927 cannot extrapolate beyond the data in the performance data. However, there were variations in the power consumption of the heat pumps during the experiment. As observed from Fig. 10b, a 50 °C water temperature was supplied to the NTES via the heat pumps, and this water was directly supplied to the greenhouse. The heat pump COP predicted by the simulation during the operation has an NSE value of 0.71, while the heat pump output water temperature at the load side has an NSE value of 0.84. Overall, the numerical prediction of

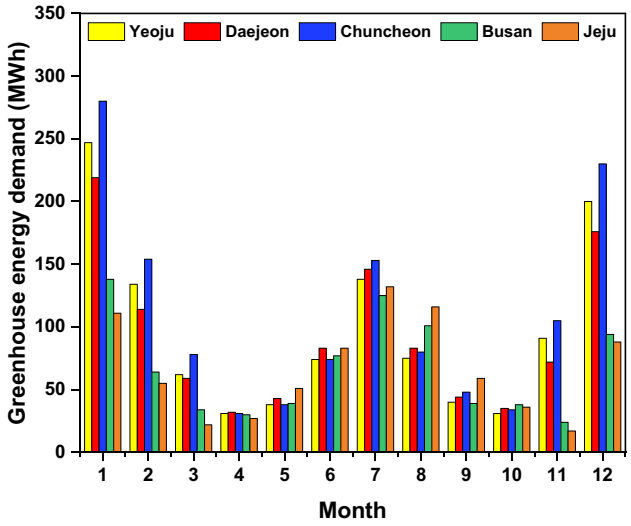

Fig. 11 Greenhouse loads in different cities in South Korea

Table 2 Yearly greenhouse load at different locations in South Korea

Cities	Heating (MWh)	Cooling (MWh)
Yeoju	774	389
Daejeon	666	440
Chuncheon	893	411
Busan	351	454
Jeju	291	509

the TRNSYS model is acceptable as the NSE value for the heap pump loop is greater than 0.5.

The heat pump primary control affects the heat pump COP and output water temperature in Fig. 10. The primary control is an on–off cycling due to the constant-speed compressor type. As opposed to the variable speed compressor that can adjust their speed, the heat pump turns on and off periodically to maintain 50 °C output water temperature.

As the comparison of all HRETESSs loop are within the recommended value for NSE, the developed TRNSYS model gained confidence and can be used as a base model for other locations in South Korea. More so, TRNSYS results are generally acceptable for preliminary investigation (Akpenpuun et al. 2022).

Thermal and electrical energy performance of the hybrid systems

The TRNSYS model is an integrated model of the HRETESSs, and the greenhouse, whose performance is dependent on the greenhouse condition. The optimum indoor climate for most crops grown in a greenhouse differs, ideally between 18 and 22 °C in winter (Semple et al. 2017) and between 30 and 35 °C in summer (Akpenpuun et al. 2021). Using the lower band of this heating and cooling setpoint temperature, the performance of the HRETESSs for different climates in South Korea was investigated.

For the greenhouse loop, the monthly variation of the greenhouse load is illustrated in Fig. 11, and the total yearly greenhouse load is presented in Table 2. Comparing Yeoju with the base case condition where the inside greenhouse temperature was varied, there was an increase of 158 and 202 MWh in the total heating and cooling load.

Figure 12 illustrates the overall thermal energy ratio encompassing both cooling and heating loads delivered to the greenhouse by each of the HRETESSs across various locations in South Korea. In Yeoju, during October, the TTES and ASHP supplied 23.8 and 7.4 MWh of thermal energy, respectively. This results in a 2.9 MWh increment in the thermal energy supplied by TTES and a 2.5 MWh reduction in the thermal energy supplied by ASHP compared to experimental results from a prior study (Kim et al. 2022). The increase in thermal energy supplied by TTES during experimentation can be attributed to the variations in the heating control temperature between the simulation (setpoint of 18 °C) and the experimental phase (ranging between 20 and 21 °C). Additionally, the decrease in ASHP-supplied thermal energy is due to its exclusive role in providing heating during experimentation, whereas it performed both heating and cooling functions in the simulation. Notably, TTES fully met the heating needs of the greenhouse in October across other cities, while it supplied an additional 55% in Busan by November.

In Jeju, no heating was required during the transition months and the ASHP supplied 27.1 and 51.2 MWh of cooling energy for the greenhouse in April and May, respectively. However, the ASHP contributed 28.6, 30.8, 24.5, and 29.9 MWh of thermal energy in April and 16.6, 15.9, 25.2, and 36.8 MWh of thermal energy in May in Yeoju, Daejeon, Chuncheon, and Busan, respectively. Despite the total thermal energy required in May being higher than in April for all cities, the ASHP's contribution was lower in May compared to April. This led to a higher contribution from HHP1, HHP2, and GSHP to the thermal energy. In April, the operation of HHP1, HHP2, and GSHP contributed a total of 2, 1, 6, and 0.4 MWh of thermal energy, respectively. In May, these systems contributed 21, 27, 12, and 2 MWh in Yeoju, Daejeon, Chuncheon, and Busan, respectively. Moreover, during the summer, the ASHP satisfied the cooling load in Chuncheon and Busan, while the GSHP contributed 28, 36, and 16 MWh to the total cooling load in Yeoju, Daejeon, and Jeju, respectively. In most of the months, the total greenhouse heating load exceeds the cooling load, except in Jeju,

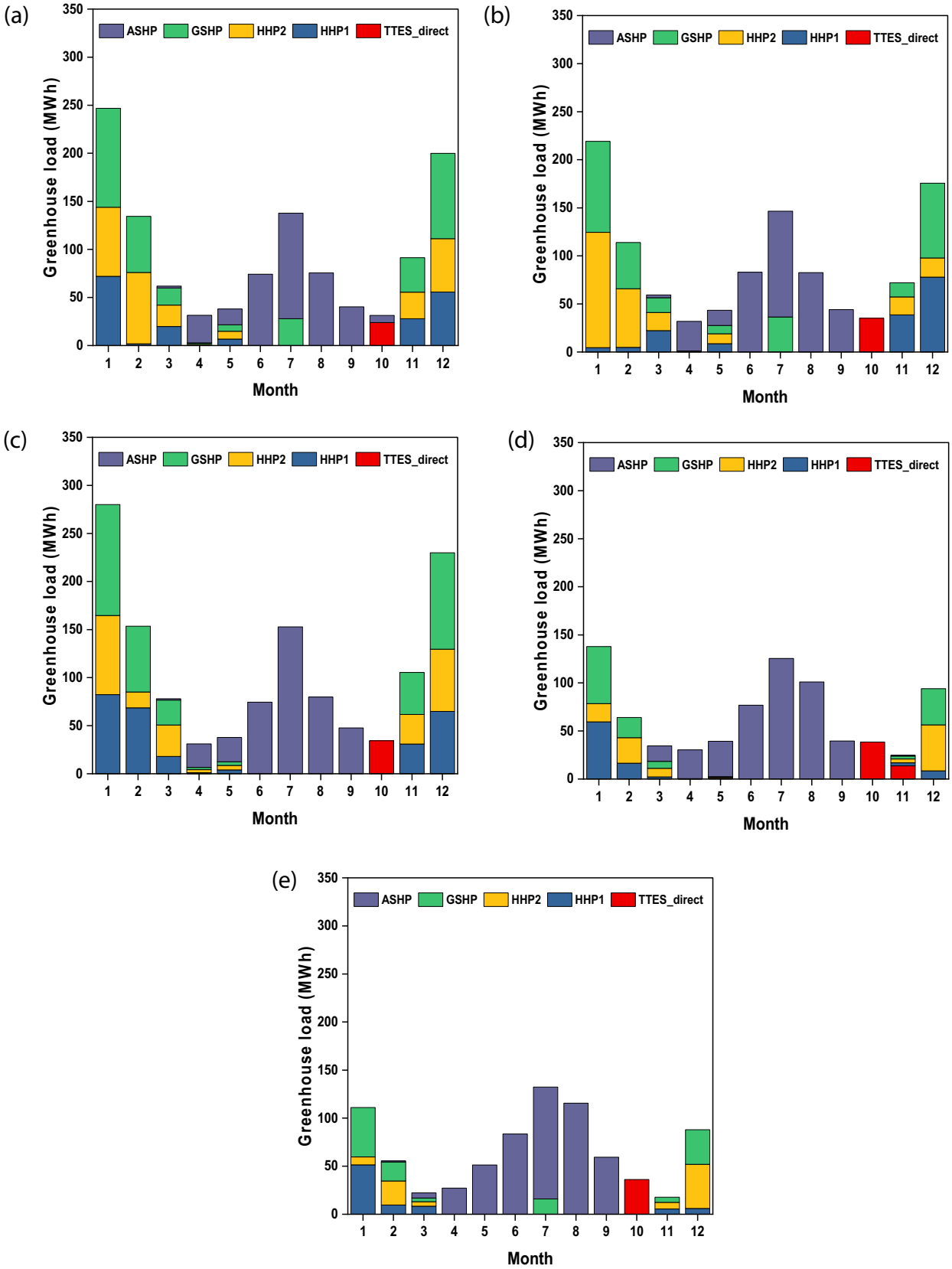

Fig. 12 Contribution of each system to the greenhouse load: **a** Yeoju, **b** Daejeon, **c** Chuncheon, **d** Busan, and **e** Jeju

where the peak average monthly low and high temperatures are 6 °C and 27.8 °C, respectively.

While investigating the contribution of each HRETESSs to the energy supplied to the greenhouse, in Yeoju, the TTES, BTES, GSHP, and ASHP accounted for 208.2 (17.9%), 261 (22.5%), 339.2 (29.2%), and 354.4 MWh (30.5%), respectively, of the total greenhouse load. In contrast with the varying setpoint temperatures during five months of experimentation, the TTES, BTES, and GSHP accounted for 124.1 (28%), 89.0 (20%), and 195.3 MWh (44%), respectively, of the heating load (Kim et al. 2023). The disparity between the simulated and experimental outcomes can be attributed to the variation in the operational timeframe of the HRETESSs, BTES condition, and heat pump operation. While the simulation is conducted for a duration of one year, the control of the heat pump system relies on heating and cooling signals from the greenhouse. Also, the BTES was neither charged by the ST nor the PVT during the first five months of heating the greenhouse as reported during the experiment. However, the charging of BTES was implemented in the simulation. Further, the ASHP contribution to the cooling load was not considered in the experimentation, and there were times the ASHP was in operation during simulation even during the heating period to keep the greenhouse temperature below 30 °C during the day.

Figure 13 shows the solar thermal fraction for various cities. In decreasing order, Busan, Jeju, Daejeon, Yeoju, and Chuncheon exhibits 57%, 56%, 38%, 30%, and 20%, respectively. As the energy demand for the varying greenhouse temperature control reduces by 158 MWh, the simulated solar fraction for Yeoju reduces from 37 to 30%. The solar fraction achieved at Jeju is comparable to the findings of Chung et al. (1998). In their study, they reported a solar fraction of 59% for Jeju using a 400-m^2 ST area and a 1000-m^3 storage volume. Also, the solar electric fraction shows a similar pattern for Busan, Jeju, Daejeon, Yeoju, and Chuncheon, exhibiting 23.4%, 20.4%, 19.1%, 19%, and 18.6%, respectively.

Figure 14 presents the flow of electrical energy to the greenhouse on July 5th in Yeoju. In the early hours before 05:00 h, there was an overlap between the greenhouse load (depicted as a solid, thick black line in Fig. 14a) and the grid output (represented by a solid blue line in Fig. 14b). During this time frame, the greenhouse's electrical energy demand is entirely met by the grid, coinciding with zero PV output power (illustrated as a dashed light black line in Fig. 14a). As the sun rises and SR increases, a notable transition occurs. The power drawn from the grid progressively diminishes, while the PV output power experiences a corresponding increase. This trend continues until the power drawn from the grid reaches a minimum of 3 kW at a specific point in time, precisely when the power generated by the PV system peaks at 29 kW. The red line in Fig. 14b visually tracks the power flow from the PV system to the battery and from the battery to the greenhouse. Positive and negative values on this line signify charging and discharging activities of the battery. A particularly intriguing observation arises

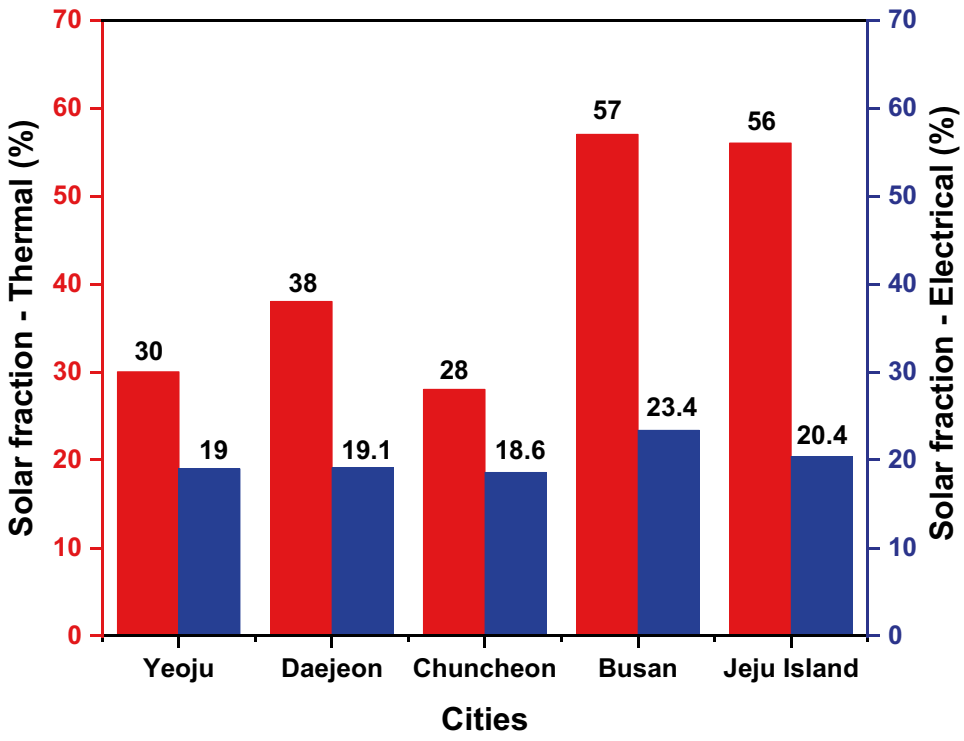

Fig. 13 Solar thermal and solar electric fractions of different cities in South Korea

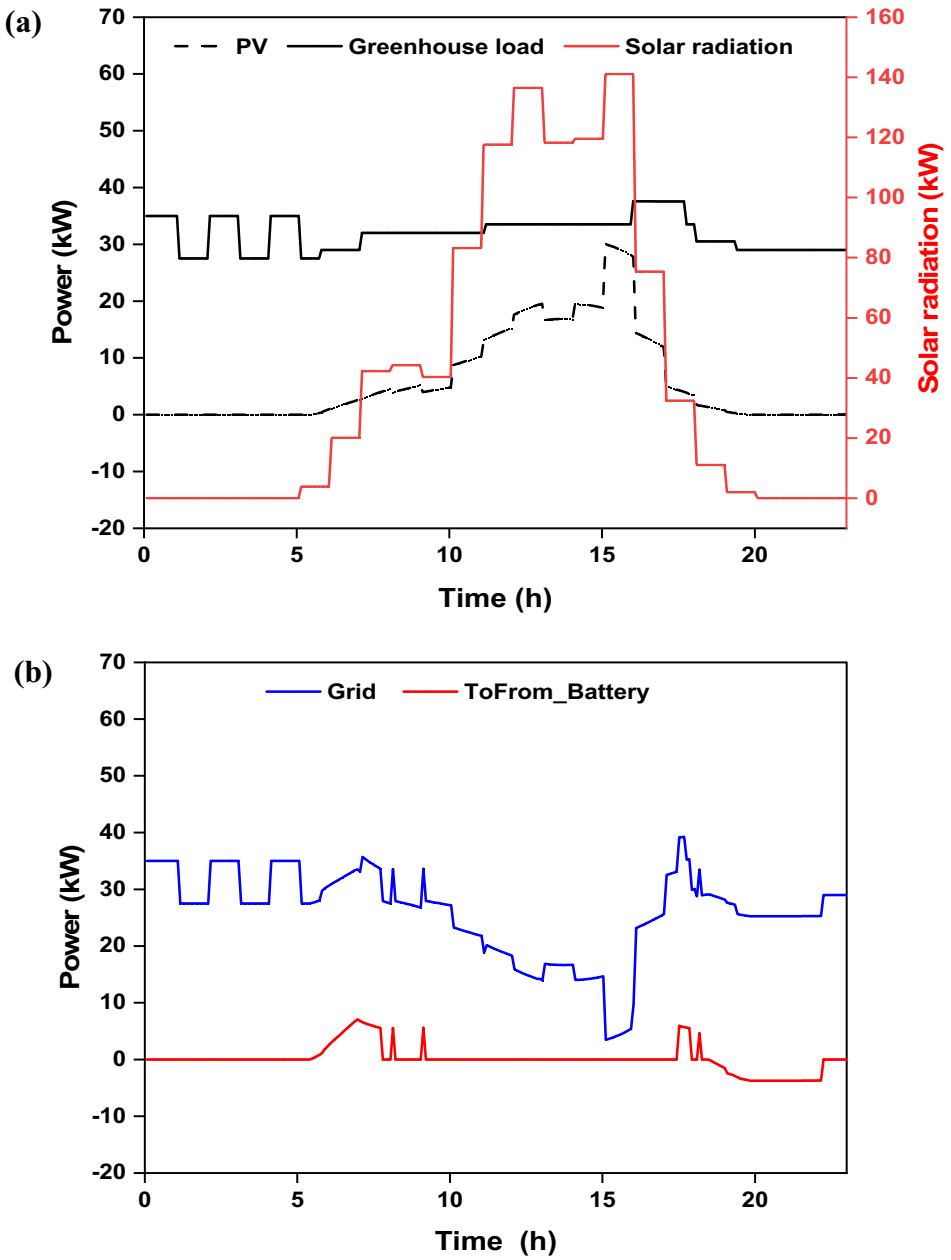

Fig. 14 Comparison of the greenhouse electric load obtained from the grid and PV

around 20:00 h on the battery line. Despite the absence of SR and therefore no power generation by the PV system, the battery supplies approximately 4 kW of energy. This serves as stored electrical energy utilization, as the battery contributes to fulfilling the greenhouse's electrical load.

Additionally, the electrical energy ratio of the investigated systems for several months is dependent on the thermal energy load, as shown in Supplementary Fig. 15. For most of the cities, the peak and low PV contributions are observed mostly in April and January during the minimum and maximum thermal energy demand. Moreover, the figure also shows that the PV provides on average 20% of the total greenhouse electrical energy demand (Fig. 15).

Effect of solar collector area and tank volume on solar fraction and collector's efficiency

A parametric study varying the ST area and TTES volume between 10 to 40% of the present system design capacity in Yeoju was conducted using TRNEdit (the TRNSYS application for editing input file). The ST loop control and greenhouse yearly load were kept unchanged for a typical one-year simulation, and the thermal energy collected from the ST collector and the thermal energy supplied from the TTES to the greenhouse under the simulation's predefined conditions were exported to an external file for further processing. There were 20 runs

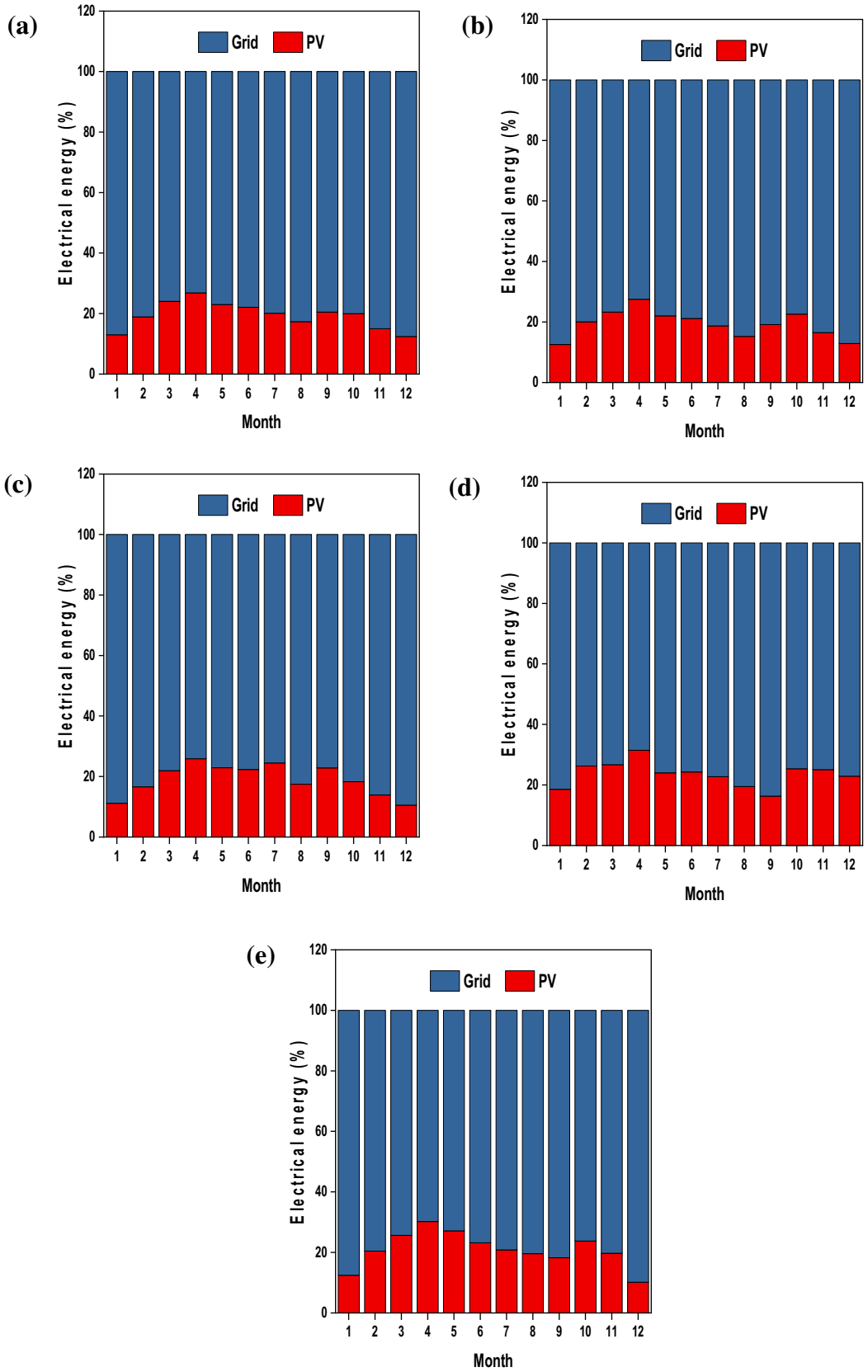

Fig. 15 Ratio of the electrical energy supplied by the PV and grid per month: (**a**) Yeoju, (**b**) Daejeon, (**c**) Chuncheon, (**d**) Busan, and (**e**) Jeju

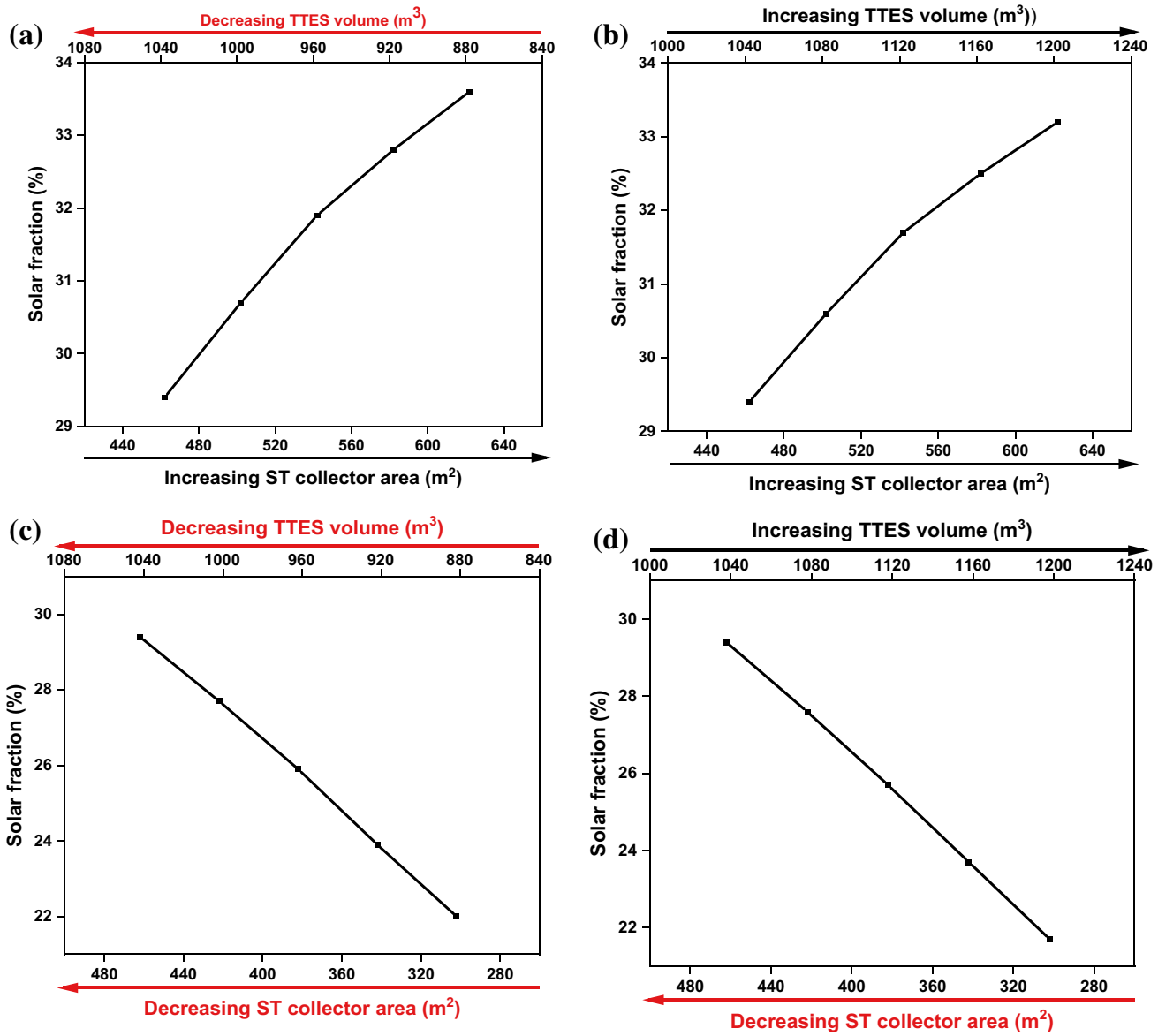

Fig. 16 Effect of solar collector area and TTES volume on solar fraction

in TRNEdit, and other simulation parameters, except for the ST collector area and TTES volume, were kept unchanged. The ST collector area and TTES volume were chosen as the parameters for optimization as they directly influence the overall performance of the solar heating system. More so, the cost of the ST collector and TTES is the highest compared to other components of the system, and optimizing their performance directly influences the overall cost of the integrated hybrid system.

Figure 16 illustrates the impact of varying the ST area and TTES volume on the solar fraction, while Fig. 17 depicts their influence on ST collector efficiency. In Fig. 16a, b, it was observed that altering the TTES volume while simultaneously increasing the ST collector area leads to an increase in the solar fraction. Similarly, Fig. 17a, b demonstrates that modifying the TTES volume, along with an increase in the ST collector area, also results in a higher solar fraction. Conversely, Fig. 16c, d reveals that adjusting the TTES volume while reducing the ST area decreases the solar fraction. Similarly, as shown in Fig. 17c, d, modifying the TTES volume while reducing the ST area reduces collector efficiency. These findings suggest that the ST area exerts a more significant influence on both solar fraction and ST efficiency compared to the TTES volume. Notably, there is a 10:1 correlation between the ST collector area and ST efficiency. Specifically, for every 10 m^2 increase in the ST area, there is a 1% improvement in the collector's efficiency. Even

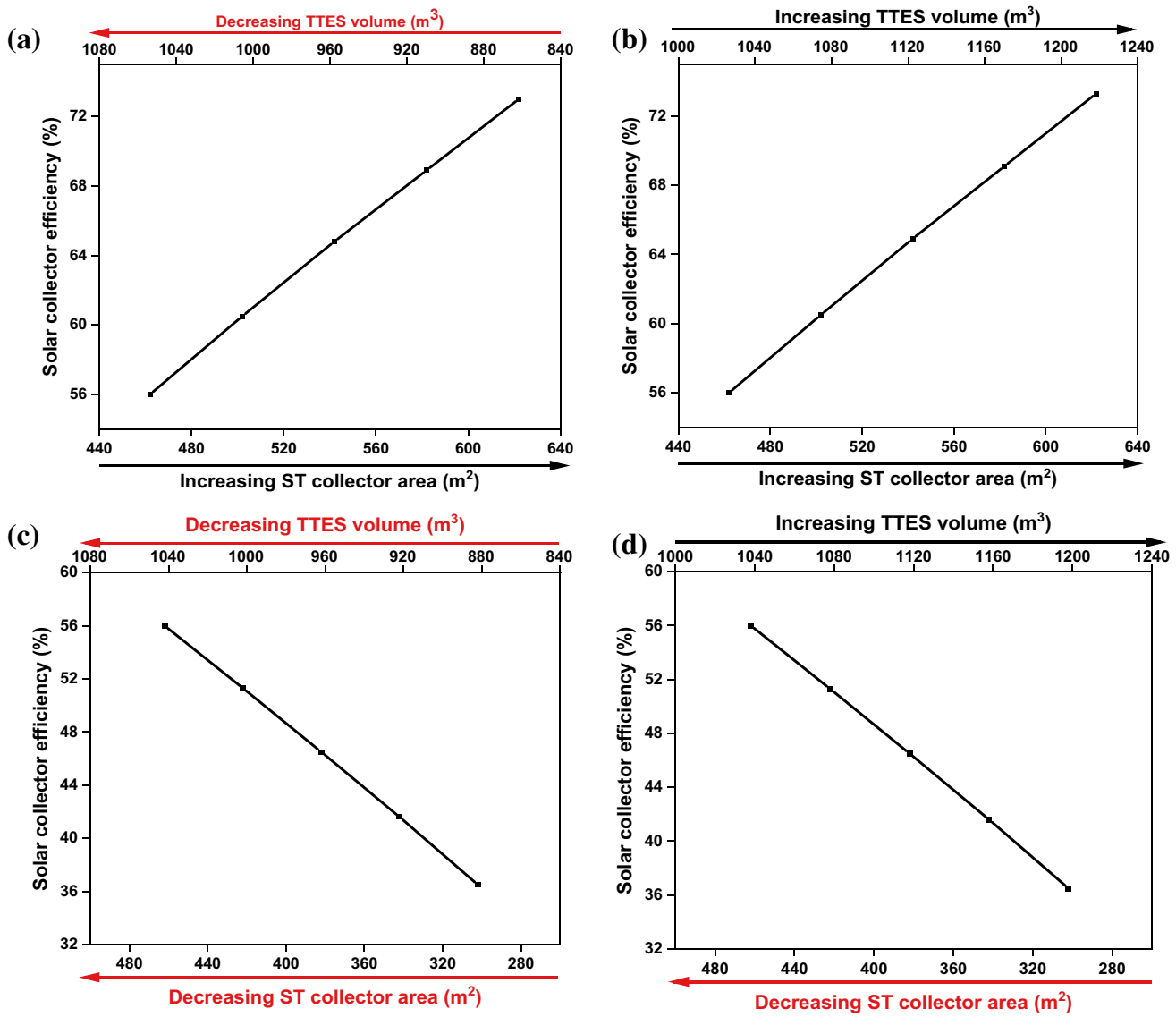

Fig. 17 Effect of solar collector area and TTES volume on solar collector's efficiency

though the value of the solar collector efficiency increases from 56.4% to 73.3% during the optimization, the solar fraction only increases from 37.1 to 42.4% due to the constant yearly energy consumption by the greenhouse in Yeoju.

Further, with a 20% increment in the TTES volume and solar collector area, there was a 0.2% reduction in the solar fraction and a 0.1% increment in the efficiency of the ST collector. The reason for the increment in the ST collector efficiency is that low water temperatures are returned to the ST collector with an increasing volume of TTES, thereby gaining more energy from the incident SR. Conversely, the solar fraction decreases because higher volume of TTES results in lower water temperatures supplied to the greenhouse. More specifically, the results show a decrease in solar fraction within the range of 1000 to 1240 m^3. This contrasts with the findings of Farooq and Zhang (2022), that reported an increase in solar fraction between 0 and 0.4 m^3, followed by a subsequent decrease between 0.4 and 1.0 m^3. The initial increase in solar fraction, as previously reported, is attributed to the corresponding rise in available thermal energy within the tank.

RETscreen Expert feasibility studies

The RETscreen Expert software was utilized to evaluate the environmental and financial feasibility of the HRETESSs,

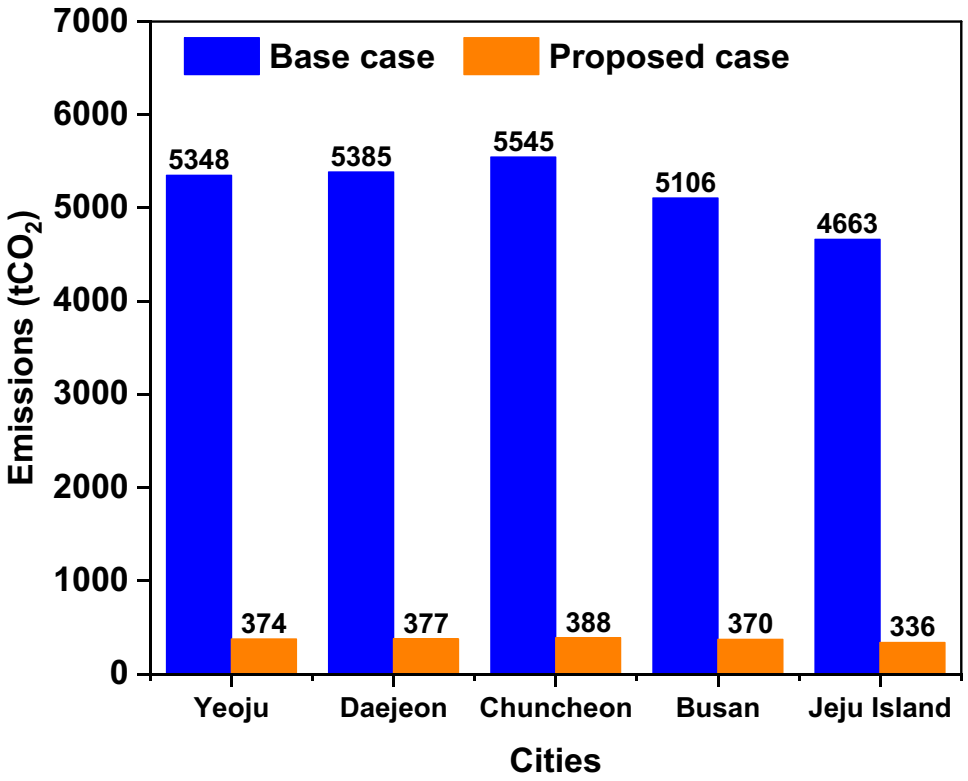

Fig. 18 Comparative analysis of GHG emissions for South Korean metropolitan cities

Table 3 Initial investment cost for each renewable energy system

Components	Cost (×1000 KRW)
Solar thermal collectors	160,000
Photovoltaic thermal collectors	448,000
Heat pumps	310,000
TTES	320,000
BTES	340,000
Buffer tank	130,000
Pipeline	250,000
System integration and control system	75,000
Total initial investment cost	2,033,00

Table 4 Financial input parameters in RETscreen

Financial inputs	Rate
Inflation rate	2%
Discount rate	5%
Project life	25 years
Debt ratio	70%
Debt interest rate	14.5%
Debt term	15 years

aiding in the identification of the optimal energy solution for the greenhouse. This assessment effectively balanced considerations of cost-effectiveness and environmental impact.

Emission analysis

Evaluating the environmental impact and cost-effectiveness of various RESs for greenhouses is essential in addressing environmental degradation and global warming, as the agricultural sector is responsible for one-third of the global GHG emission (Gilbert 2012). Figure 18 illustrates the emission reduction for Yeoju and other cities, with Jeju achieving the least GHG emission reduction, followed by Busan, Yeoju, Daejeon, and Chuncheon.

As of 2022, the GHG credit rate in South Korea was 35,000 KRW/tCO_2 (Kim et al. 2022), which is equivalent to 26.2 \$/tCO_2, and trading the amount of emission reduction at 10% credits transaction, the result for the different location is presented in Fig. 19. The results indicate that 133,7600, 129,900, 129,020, 122,840, and 112,230 dollars can be generated from Chuncheon, Daejeon, Yeoju, Busan, and Jeju, respectively. This revenue is being deducted from the NPV and annual life savings (ALS) in the RETscreen software and contributed to the reduced payback period of the project in all the locations.

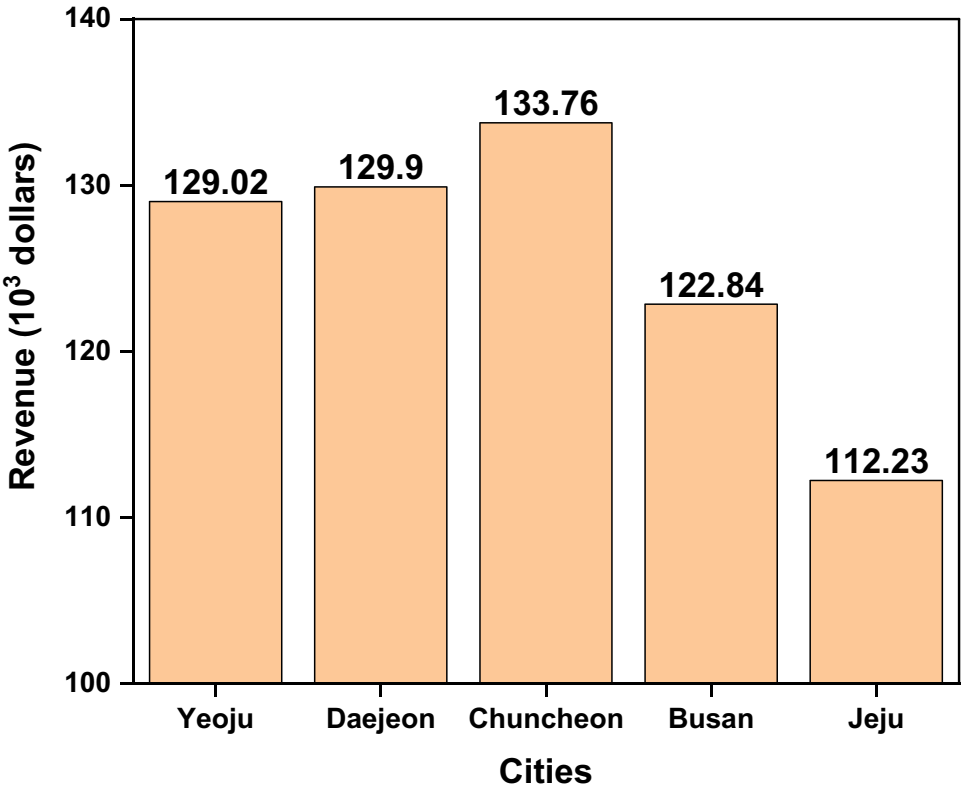

Fig. 19 Carbon trading revenue through GHG emission reduction

Financial analysis

To figure out if the HRETESSs was financially feasible, a number of factors were looked at. These included the initial cost, the cost of operation and maintenance (O&M), and variables such as the inflation rate, discount rate, project life, debt ratio, debt interest rate, and debt term. The initial cost of the individual components of HRETESSs is presented in Table 3, while the financial input variables, based on our assumptions, are provided in Table 4.

The O&M cost was determined to be 10% of the total initial investment cost. Using these parameters, the RETscreen simulation generated results for the ALS, IRR, NPV, benefit-cost (B-C) ratio, and levelized cost of energy (LCOE) for the project, as shown in Table 5.

The positive NPV, representing the disparity between the present value of cash inflows and outflows across all locations over a specific period, demonstrates the financial and economic feasibility of the project. Additionally, the IRR surpasses the project's required rate of return, indicating the project's economic viability across all locations. Moreover, the results indicate that the LCOE falls within the range of 0.08 to 0.207 $/kWh.

Figure 20 illustrates a comparison of the simple payback period and equity payback period of the proposed system. The equity payback period represents the point at which there is no profit or loss, indicating a breakeven situation. On the other hand, the simple payback period refers to the time required for the project to recover the initial investment made in the project (Luqman et al. 2023). Chuncheon has the least simple payback period of 6 years due to its potential to generate more revenue from CO_2 reduction, while the simple

Table 5 Financial metrics for the five locations

Financial parameters	Yeoju	Daejeon	Chuncheon	Busan	Jeju Island
NPV ($)	2,832,560	3,198,627	1,158,998	2,240,813	1,443,437
IRR (%)	21.5	23.1	13.4	19	14
ALS ($)	310,297	350,398.38	126,964.23	245,473.19	158,123.52
B–C ratio (%)	2.4	2.6	1.5	2.1	1.6
LCOE ($)	0.088	0.080	0.092	0.102	0.207

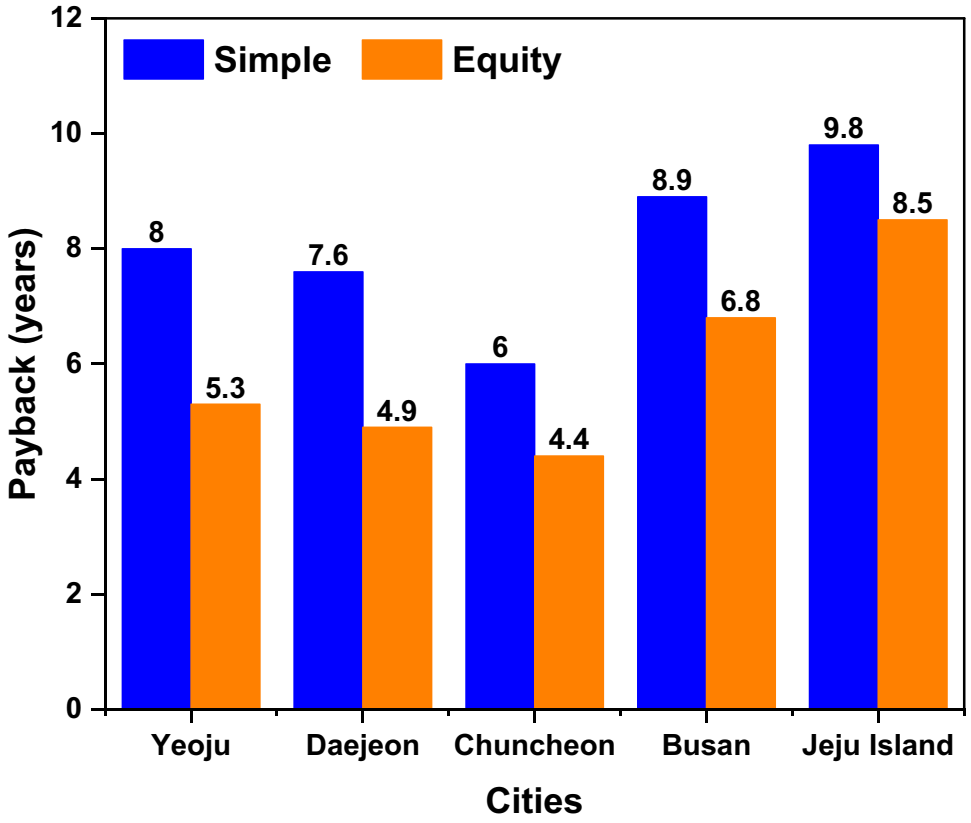

Fig. 20 Payback period for the five locations

Table 6 Sensitivity analysis of the project

Debt interest rate (%)	Initial costs ($)					
	6,825,000	7,962,500	9,100,000	10,237,500	11,375,00	
	− 25.0	− 12.5	0.0	12.5	25.0	
5.2	− 25.0	25.1	19.2	14.7	11.3	8.4
6.13	− 12.5	24.0	18.1	13.7	10.2	7.5
7.00	0.0	22.8	17.0	12.6	9.2	6.5
7.88	12.5	21.6	15.9	11.6	8.2	5.5
8.75	25	20.4	14.7	10.5	7.2	4.5
Debt ratio (%)	Initial costs ($)					
	6,825,000	7,962,500	9,100,000	10,237,500	11,375,00	
	− 25.0	− 12.5	0.0	12.5	25.0	
53	− 25.0	18.5	14.4	11.3	8.7	6.6
61	− 12.5	20.3	15.5	11.9	8.9	6.5
70	0.0	22.8	17.0	12.6	9.2	6.5
79	12.5	27.0	19.2	13.8	9.6	6.4
88	25	35.8	23.5	15.6	10.2	6.3

payback period for Jeju has the highest value of 9.8 years with the least revenue from CO_2 reduction. Similarly, Jeju also has the longest equity payback period, at 8.5 years, while Daejeon has the shortest period, at 4.9 years. This means that the project will attract attention for 20.1 years in Daejeon and 16.5 years in Chuncheon during the project's 25-year lifespan.

Sensitivity analysis

To assess the impact of various parameters on the financial variables, a sensitivity analysis was conducted by adjusting factors such as the debt ratio and debt interest rate. This analysis focused solely on the real-life project implemented at the experimental site in Yeoju (the base case). Within the sensitivity analysis, the pretax IRR on equity was evaluated. The IRR, which excludes income tax, is the actual interest yield that the project's equity has produced over its lifetime. It is calculated based on pretax yearly cash flows and the project's duration. Comparing the IRR to an organization's required rate of return allows for the determination of the project's financial acceptability. During the sensitivity analysis, the debt interest rate and debt ratio were iterated against the initial cost, considering a sensitivity range of ± 25% and a threshold of 18%. Table 6 illustrates that if the project's initial cost increases by 25% while the debt interest rate decreases by the same percentage, the pretax IRR on equity diminishes to 8.4%, rendering the project financially unviable. Conversely, if the debt ratio increases by 25% and the initial cost decreases by 25%, the project becomes economically feasible, yielding an IRR on equity of 20.4%. Notably, the initial cost and debt ratio have a more significant impact on the project's financial viability compared to the debt interest rate. The sensitivity analysis further indicates that the IRR is most sensitive to changes in the initial cost compared to other parameters evaluated. Overall, the IRR indicator offers an advantage as it is not reliant on a discount rate specific to a particular organization, making it applicable to all project investors.

Summary and conclusions

Highlighting the importance of creating cities that are resilient and sustainable while still having a small carbon footprint is particularly important in the agricultural sector. With the current energy policy in South Korea, this study holistically investigates the performance of HRETESSs for greenhouse operations in five different cities using a base case scenario. The major findings are as follows:

- In all the cities, the ASHP had the highest contribution to the greenhouse energy load because it was the only heat pump used during the cooling period, and its performance was better in Chuncheon and Busan.
- The BTES contribution to the greenhouse load in the simulation was higher than the experimentally measured value due to heat injection from the ST and PVT.
- In the southern part of the country, Busan and Jeju had a higher solar electric fraction because the region possessed a warmer winter climate, which facilitated the high performance of the PV system even at the same electric load as other cities.
- Across all cities, the PV system, on average, fulfils 20% of the total electrical energy demand of the greenhouse.
- The parametric study on the solar thermal system indicates that the ST collector area has more influence on the solar fraction and ST efficiency compared to the TTES volume.
- Jeju Island has the highest LCOE due to its low energy demand, and the simple payback increases as the total revenue from carbon reduction decreases.
- The initial cost has a greater impact on the IRR compared to the debt ratio and debt interest rate, indicating that changes in the initial cost have a more pronounced effect on the IRR.

Supplementary Information The online version contains supplementary material available at https://doi.org/10.1007/s10098-023-02656-3.

Author contributions MAA contributed to writing, software, methodology, formal analysis, and validation. AOY contributed to writing, software, and formal analysis. AR contributed to data curation, writing, and formal analysis. ABO contributed to software and validation. QOO contributed to data curation, formal analysis, and reviewing and editing. AY contributed to writing, software, and formal analysis. W-HN contributed to visualization and investigation. M-HK contributed to conceptualization, methodology, and resources. H-TK contributed to investigation and supervision. H-WL contributed to investigation, supervision, funding acquisition, and reviewing and editing.

Funding This study was supported by the Korea Institute of Planning and Evaluation for Technology in Food, Agriculture, Forestry, and Fisheries (IPET) through the Agriculture, Food, and Rural Affairs Convergence Technologies Program for Educating Creative Global Leaders, funded by the Ministry of Agriculture, Food and Rural Affairs (MAFRA) (717001-7). Moreover, this study was supported by the Basic Science Research Program through the National Research Foundation of Korea (NRF), funded by the Ministry of Education (NRF-2019R1I1A3A01051739), and by the Korea Institute of Planning and Evaluation for Technology in Food, Agriculture and Forestry (IPET) through Agricultural Energy Self-Sufficient Industrial Model Development Program, funded by the Ministry of Agriculture, Food and Rural Affairs (MAFRA) (120096-3).

Data availability The authors do not have the permission to share the data used for this study. All the figures in this file were created using Origin software, Microsoft PowerPoint, and Surfer.

Declarations

Conflict of interest There are no conflicts of interest to declare with respect to authorship, research, and/or publication of this article.

References

Adesanya MA, Na W, Rabiu A et al (2022) TRNSYS simulation and experimental validation of internal temperature and heating

demand in a glass greenhouse. Sustainability 14:8283. https://doi.org/10.3390/su14148283
Akpenpuun TD, Na WH, Ogunlowo QO et al (2021) Effect of greenhouse cladding materials and thermal screen configuration on heating energy and strawberry (Fragaria ananassa var. "seolhyang") yield in winter. Agronomy. https://doi.org/10.3390/agronomy11122498
Akpenpuun TD, Ogunlowo QO, Rabiu A et al (2022) Building energy simulation model application to greenhouse microclimate, covering material and thermal blanket modelling: a review, Nigerian. J Technol Dev 19:276–286. https://doi.org/10.4314/njtd.v19i3.10
Alsantali MH, Almarshoud AF (2023) The economic feasibility of utilizing small-scale solar PV systems in the residential sector based on Saudi regulations. Clean Technol Environ Policy 25:889–907. https://doi.org/10.1007/s10098-022-02410-1
Anifantis AS, Colantoni A, Pascuzzi S (2017) Thermal energy assessment of a small scale photovoltaic, hydrogen and geothermal stand-alone system for greenhouse heating. Renew Energy 103:115–127. https://doi.org/10.1016/j.renene.2016.11.031
Calise F, Cappiello FL, Cimmino L, Vicidomini M (2023) Dynamic modelling and energy, economic, and environmental analysis of a greenhouse supplied by renewable sources. Appl Sci (switzerland). https://doi.org/10.3390/app13116584
Chaima E, Lian J, Ma C et al (2023) Long-term electricity demand scenarios for Malawi's electric power system. Energy Sustain Dev 73:23–38. https://doi.org/10.1016/j.esd.2023.01.012
Chew YE, Gan ZW, Heng H et al (2023) Carbon emissions pinch analysis (CEPA) for emissions reduction and energy planning in Canada. Clean Technol Environ Policy 25:2413–2431. https://doi.org/10.1007/s10098-023-02537-9
Choi G, Heo E, Lee CY (2018) Dynamic economic analysis of subsidies for new and renewable energy in South Korea. Sustainability (switzerland) 10:1–19. https://doi.org/10.3390/su10061832
Chung M, Park JU, Yoon HK (1998) Simulation of a Central Solar Heating system with Seasonal Storage in Korea. Sol Energy 64:163–178. https://doi.org/10.1016/S0038-092X(98)00101-7
Datta U, Kalam A, Shi J (2020) The economic prospect of rooftop photovoltaic (PV) system in the commercial buildings in Bangladesh: a case study. Clean Technol Environ Policy 22:2129–2143. https://doi.org/10.1007/s10098-020-01963-3
de Ridder F, van Roy J, de Schutter B, Mazairac W (2020) Seasonal energy storage for greenhouse production. Acta Hortic 1296:747–752. https://doi.org/10.17660/ACTAHORTIC.2020.1296.94
De Soto W, Klein SA, Beckman WA (2006) Improvement and validation of a model for photovoltaic array performance. Sol Energy 80:78–88. https://doi.org/10.1016/j.solener.2005.06.010
Duffie JA, Beckman WA (1982) Solar engineering of thermal processes. 4th ed. John Wiley & Sons; 2013 [Chapter 23 - Design of Photovoltaic Systems]
Engler N, Krarti M (2022) Optimal designs for net zero energy controlled environment agriculture facilities. Energy Build 272:112364. https://doi.org/10.1016/j.enbuild.2022.112364
Farooq AS, Zhang P (2022) Technical assessment, economic viability, and environmental impact of a solar-driven integrated space and water heating system in various configurations. Energy Sustain Dev 71:330–340. https://doi.org/10.1016/j.esd.2022.10.002
Gilbert N (2012) One-third of our greenhouse gas emissions come from agriculture. Nature. https://doi.org/10.1038/nature.2012.11708
Gorjian S, Calise F, Kant K et al (2021) A review on opportunities for implementation of solar energy technologies in agricultural greenhouses. J Clean Prod. https://doi.org/10.1016/j.jclepro.2020.124807
Hellstrom G (1989) Duct ground heat storage model manual for computer code. 49
Jiang W, Jin Y, Liu G et al (2023) Net-zero energy optimization of solar greenhouses in severe cold climate using passive insulation and photovoltaic. J Clean Prod 402:136770. https://doi.org/10.1016/j.jclepro.2023.136770
Kim D, Kim M-H, Lee D-W (2022) Economic and environmental analysis of solar thermal and seasonal thermal energy storage based on a renewable energy conversion system for greenhouses. Energies (basel) 15:6592. https://doi.org/10.3390/en15186592
Kim M-H, Kim D, Lee D-W, Heo J (2023) Energy conservation performance of a solar thermal and seasonal thermal energy storage-based renewable energy convergence system for glass greenhouses. Case Stud Therm Eng 44:102895. https://doi.org/10.1016/j.csite.2023.102895
KMA (2023) Weather Data Opening Portal. https://data.kma.go.kr/data/grnd/selectAsosRltmList.do?pgmNo=36. Accessed 18 Jun 2022
Lee JY (2009) Current status of ground source heat pumps in Korea. Renew Sustain Energy Rev 13:1560–1568. https://doi.org/10.1016/j.rser.2008.10.005
Lee J, Xydis G (2023) Floating offshore wind projects development in South Korea without government subsidies. Clean Technol Environ Policy. https://doi.org/10.1007/s10098-023-02564-6
Lee CG, Cho LH, Kim SJ et al (2021) Comparative analysis of combined heating systems involving the use of renewable energy for greenhouse heating. Energies (basel). https://doi.org/10.3390/en14206603
Luqman R, Kehinde Issa A-J, Owolabi AB et al (2023) Assessing the viability of a grid-connected PV power plant in Mubi, Adamawa State, Nigeria. Front Energy Res 11:2023. https://doi.org/10.3389/fenrg.2023.1205646
MOTIE (2017) Korea's renewable energy 3020 plan
Nadi F, Campbell D (2023) Assessment of the thermodynamic, environmental and economic output of agro-ecosystems: onion set versus onion production. Clean Technol Environ Policy 25:1223–1240. https://doi.org/10.1007/s10098-022-02439-2
Ogunlowo QO, Na WH, Rabiu A et al (2022) Effect of envelope characteristics on the accuracy of discretised greenhouse model in TRNSYS. J Agric Eng. https://doi.org/10.4081/jae.2022.1420
Ouazzani Chahidi L, Mechaqrane A (2023) Energy and economic analysis for the selection of optimal greenhouse design: a case study of the six Morocco's climatic zones. Energy Build 289:113060. https://doi.org/10.1016/j.enbuild.2023.113060
Owolabi AB, Nsafon BEK, Huh JS (2019) Validating the techno-economic and environmental sustainability of solar PV technology in Nigeria using RETScreen Experts to assess its viability. Sustain Energy Technol Assess 36:100542. https://doi.org/10.1016/J.SETA.2019.100542
Pan Y, Liu L, Zhu T et al (2017) Feasibility analysis on distributed energy system of Chongming County based on RETScreen software. Energy 130:298–306. https://doi.org/10.1016/j.energy.2017.04.082
Semple L, Carriveau R, Ting DSK (2017) A techno-economic analysis of seasonal thermal energy storage for greenhouse applications. Energy Build 154:175–187. https://doi.org/10.1016/j.enbuild.2017.08.065
Solar Energy Laboratory Univ of W-M (2018) Trnsys 18. Solar energy laboratory, vol 2. University of Wisconsin-Madison, pp 7–36
Tremblay O, Dessaint LA, Dekkiche AI (2007) A generic battery model for the dynamic simulation of hybrid electric vehicles. In: VPPC 2007—proceedings of the 2007 IEEE vehicle power and propulsion conference, pp. 284–289. https://doi.org/10.1109/VPPC.2007.4544139
Ushamah HM, Ahmed N, Elfeky KE et al (2022) Techno-economic analysis of a hybrid district heating with borehole thermal storage for various solar collectors and climate zones in Pakistan. Renew Energy 199:1639–1656. https://doi.org/10.1016/j.renene.2022.09.059

Wikipedia (2021) Variation of temperature in South Korea. https://en.wikipedia.org/wiki/South_Korea#Geography,_climate_and_environment. Accessed 11 Nov 2021

Yakub AO, Same NN, Owolabi AB et al (2022) Optimizing the performance of hybrid renewable energy systems to accelerate a sustainable energy transition in Nigeria: a case study of a rural healthcare centre in Kano. Energt Strategy Rev 43:100906. https://doi.org/10.1016/j.esr.2022.100906